Photodisintegration of ^{3}H and ^{3}He

D. D. Faul, B. L. Berman, P. Meyer, and D. L. Olson
Lawrence Livermore Laboratory, University of California, Livermore, California 94550
(Received 18 August 1980)

The photoneutron cross sections for ^{3}H and ^{3}He have been measured from threshold to $\sim$25 MeV with monoenergetic photons from the annihilation in flight of fast positrons. These reactions include the two-body breakup of ^{3}H and the three-body breakup of both ^{3}H and ^{3}He; these measurements for ^{3}H are the first to span the energy region across the peaks of the cross sections. An efficient BF_3-tube-and-paraffin neutron detector and high-pressure gaseous samples were employed in these measurements. The results, when compared with each other and with results for the two-body breakup cross section for ^{3}He from the literature, show that: (a) the two-body breakup cross sections for ^{3}H and ^{3}He have nearly the same shape, but the one for ^{3}He lies lower in magnitude; (b) the three-body breakup cross section for ^{3}He lies higher in magnitude, broader in the peak region, and also rises less sharply from threshold than that for ^{3}H; and (c) these differences between the cross sections for the breakup modes largely compensate in their sum, so that the total photon absorption cross sections for ^{3}H and ^{3}He are nearly the same in both size and shape at energies near and above their peaks. Theoretical results from the literature disagree with the experimental results to a certain extent over the entire photon-energy region for which the photoneutron cross sections were measured. Sum rule predictions also fail to reproduce the experimental results. These discrepancies constitute a challenge to the principle of charge symmetry of the nuclear force, but more complete theoretical calculations are needed to ascertain whether these discrepancies can be ascribed entirely to electromagnetic effects.

[NUCLEAR REACTIONS ^{3}H(γ,n), ^{3}H(γ,2n), ^{3}He(γ,n); measured $\sigma(E_\gamma)$, threshold to $\sim$25 MeV; monoenergetic photons, high-pressure gas samples; two-body breakup, three-body breakup, charge asymmetry.]

I. INTRODUCTION

This paper reports a measurement of three of the four possible photodisintegration cross sections for the two $T = \frac{1}{2}$ three-body nuclei, ^{3}H and ^{3}He, from threshold to <30 MeV. For ^{3}H the reactions measured were ^{3}H(γ,n)^{2}H ($Q = -6.257$ MeV) and ^{3}H(γ,2n)^{1}H ($Q = -8.482$ MeV), while for ^{3}He the reaction ^{3}He(γ,n)2p ($Q = -7.718$ MeV) was measured. The photodisintegration channel not measured in this investigation is ^{3}He(γ,d)^{1}H ($Q = -5.493$ MeV).

A general discussion of the structures of ^{3}H and ^{3}He can be found in the review article of Levinger.[1] Although they are mirror nuclei, ^{3}H and ^{3}He differ in several ways, including the static Coulomb repulsion between the two protons in ^{3}He (which contributes about 0.640 MeV to the total 0.764-MeV reduction of its binding energy),[2,3] the instability of ^{3}H (which β decays to ^{3}He with a half-life of 12.26 yr), and their charge radii [1.70 $\pm$ 0.05 fm for ^{3}H (Ref. 4) and 1.935 $\pm$ 0.03 fm for ^{3}He (Ref. 5)]. Since the ground state of the trinucleon system is dominated by the totally symmetric S term (although nine different terms are permitted),[6,7] the continuum resulting from a dipole photon interacting with a stable trinucleon is dominated by a single partial wave ($l = 1$). Further discussion of electromagnetic interactions involving ^{3}H and ^{3}He can be found in the review articles of Gorbunov,[8] Weiss,[9] and Ciofi degli Atti.[10]

Similarity of the two trinucleons, except for electromagnetic (Coulomb) effects, would be a consequence of the principle of the charge symmetry of

the nuclear (strong) force, which says that the strong interaction between two protons is identical to that between two neutrons. Therefore, any experimental difference of ^{3}He from ^{3}H which cannot be obtained as a consequence of the electromagnetic interaction is a measure of charge-symmetry breaking in the nucleon-nucleon force. The present measurement of the photoneutron cross sections for both ^{3}H and ^{3}He allows two new comparisons between mirror reactions. The comparisons between the three-body breakup reactions of ^{3}He and ^{3}H is the stronger because it is obtained entirely from the results of these measurements, thus reducing the chance for systematic errors.

A. Previous experimental work

The two-body photodisintegration cross section for ^{3}He has been measured in many experiments. Several used incident photon beams produced either by electron bremsstrahlung[11–17] or by proton capture on CaF_2.[18] In other measurements the cross section for the ^{3}He(γ,d) reaction was deduced from electrodisintegration data.[19–22] The ^{3}He two-body cross section also has been determined using detailed balance either with a proton capturing a deuteron or vice versa.[23–29]

Only three previous measurements of the three-body breakup cross section of ^{3}He have been reported in the literature: Gorbunov *et al.*[12] used bremsstrahlung and ^{3}He gas in a cloud chamber to measure ^{3}He(γ,2p)n from threshold to 170 MeV; Gerstenberg and O'Connell[30] used bremsstrahlung and a liquid sample to measure ^{3}He(γ,n)2p from threshold to 30 MeV; and Berman *et al.*[31] used monoenergetic photons and a liquid sample to make a second measurement of ^{3}He(γ,n)2p from threshold to 30.2 MeV.

Three previous measurements of the photodisintegration of tritium have been reported in the literature.[32–34] None, however, has yielded the two-body breakup cross section at its peak. Bösch *et al.*[33] used a nuclear reactor to produce an intense source of neutron-capture γ rays (10^6 cm^{-2} sec^{-1}) and a 15-Ci ^{3}H-gas sample (at 10 atm). Pfeiffer and collaborators[34] used bremsstrahlung photons (endpoint energy 32.5 MeV) and a gaseous ^{3}H sample (200 Ci at 0.55 atm). There also was an early measurement of the capture cross section for 14.4-MeV neutrons on ^{2}H reported by Cerineo *et al.*[32] A single datum for the ^{3}H(γ,2n) cross section at 10.8 MeV also is reported in Ref. 33; and the proton spectrum from the three-body photodisintegration of tritium (but no three-body breakup cross section) is reported in Ref. 34. No other measurement of the three-body photodisintegration cross section for ^{3}H has been reported.

B. Previous theoretical work

Early theoretical treatments of the photodisintegration of the trinucleons include that of: (a) Verde,[35] who confirmed that the matrix element of an $M1$ transition from the ground state to the two-body continuum vanishes[36] and who calculated the 90° differential cross sections for the two-body photodisintegration of ^{3}H and ^{3}He using a Gaussian ground-state wave function and a final-state wave function composed of a plane-wave nucleon and a deuteron bound by the Yukawa potential; (b) Gunn and Irving,[37] who calculated both the two- and three-body total photodisintegration cross sections using an exponential form for the ground-state wave function, which had a more realistic asymptotic behavior than that used by Verde, but not including final-state interactions; (c) Eichmann,[38] who calculated the two-body breakup using a Gunn-Irving ground state modified by an admixture of the mixed-symmetry S' term (which arises from the nucleon-nucleon tensor force) and both electric dipole and quadrupole excitations, but no final-state interactions; and (d) Rahman *et al.*,[39] who calculated the ^{3}H(γ,n) cross section using a modified Gunn-Irving initial state (whose parameters are fixed by a simple variational procedure) and a final-state wave function which reproduces the $l = 1$ n-d phase-shift data, but no coupling to the three-body channel.

In order to delineate more fully the effects of the final-state ineractions, e.g., the enhancement of the two-body cross section over the plane-wave result even though the $l = 1$ n-d phase shift is very small, a more exact theoretical treatment is required. Such a calculational method is that of Faddeev,[40] and the model potential usually employed is, as first proposed by Mitra,[41] a separable potential of the Yamaguchi type.[42] Model calculations using these techniques also can account consistently (within the model) for the three-body bound-state wave function (as well as for the multiple rescattering effects in the final state). Several such calculations of the photodisintegration cross sections for the trinucleons have been performed.[43–49]

In addition to the Faddeev-type calculations, which are exact within the model assumed for the

nucleon-nucleon interaction, several more approximate theoretical calculations using the method of hyperspherical harmonics have been performed.[50–53] This method employs a transformation from the conventional Jacobian variables (see Ref. 35) to a set of new variables which reduces the calculational problem to two one-dimensional second-order differential equations for both the ground state and the continuum.

II. EXPERIMENTAL METHODS AND PROCEDURES

The general features, as well as many specific details, of the apparatus and procedures used for measuring photoneutron cross sections at the Lawrence Livermore Laboratory Electron-Positron Linear Accelerator (LINAC) have appeared elsewhere in the recent literature.[54,55] The cross section σ at a given photon energy is calculated from an expression of the form

$$\sigma = (n/q)^{\text{net}}(q/a)(\text{saf})g(1/\epsilon) , \quad (1)$$

where q/a is the number of photon-flux monitor units per annihilation photon; saf (the solid-angle factor) is the constant (for a given nuclear sample) which contains (i) the ratio of the solid angles subtended at the annihilation target by the NaI(Tl) spectrometer used to calibrate the photon-flux monitor and by the collimator which defines the beam which strikes the sample and (ii) the effective number of sample atoms per unit area that are irradiated; $g = \mu t(1 - e^{-\mu t})$, where μ is the photon linear-attenuation coefficient for the sample and t is the sample thickness; and ϵ is the effective neutron detector efficiency. The net neutron yield per photon-flux monitor unit $(n/q)^{\text{net}}$ is obtained from

$$(n/q)^{\text{net}} = [(n/q)_s^+ - k(n/q)_s^-] - m[(n/q)_{sb}^+ - k(n/q)_{sb}^-] , \quad (2)$$

where the superscripts $\pm$ indicate $e^\pm$ beams, k is the normalization constant which accounts for the different responses of the ionization chamber to the distinct photon spectra produced by the $e^\pm$ beams, and m is the constant which normalizes the separate measurement of the sample-blank (sb) yield rate to the actual yield rate of the sample container holding the sample(s).

A. The annihilation-photon beam

A detailed diagram of the experimental apparatus following the annihilation target is shown in Fig. 1. The collimator and NaI(Tl) crystal which are indicated with dashed lines in Fig. 1 were in place only for the runs in which the ionization chamber was being calibrated (see below). A discussion of the energy, angular spread, and the resolution of the quasimonoenergetic photon beam is given in Ref. 55.

In order to produce beams of annihilation photons, a high-current, $\sim$130-MeV electron beam (200 μA time averaged, having a pulse rate of 300 Hz and a pulse width of 3 μsec) from the LINAC is focused onto a tungsten-rhenium converter target. The positrons from the converter target, which is 2.5 radiation lengths thick, are passed through a series of bending and focusing magnets and an energy-analyzing slit which resolves the momentum of the beam to $\pm 1\%$. After being analyzed, typical average positron currents are 1 nA at 24 MeV and 0.5 nA at 12 MeV. The positrons then are focused onto a beryllium disk (12.7 mm in diameter and 0.76 mm in thickness) in which a small fraction annihilates with the atomic electrons. That (large) fraction of the positrons which passes through the beryllium target without annihilating is swept mag-

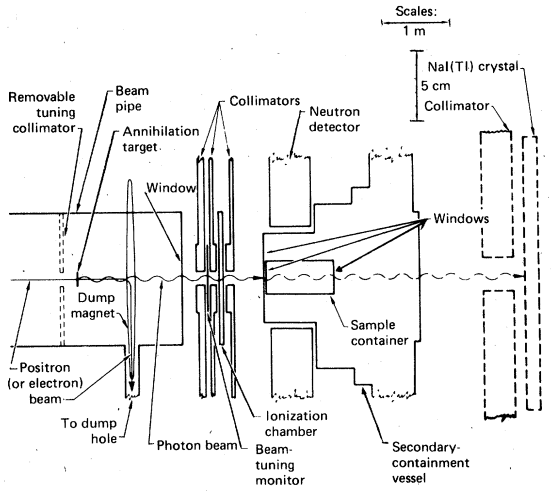

FIG. 1. Schematic diagram of the experimental layout for the present measurements with gas samples. Note the different horizontal and vertical scales. The NaI(Tl) crystal and its collimator (drawn with dashed lines) are installed only when the ionization chamber is being calibrated. Shielding has been omitted for clarity.

netically, by 90°, out of the photon beam line and into a 5-m-deep well.

The energy calibration of the annihilation-photon beam was verified to 0.25% by the observed location of several photoneutron thresholds. The resolution (FWHM) of the beam ranged from approximately 220 keV at $E_\gamma = 5$ MeV to 505 keV at $E_\gamma = 30$ MeV. The method by which this energy calibration and the resolution were determined also is discussed in Ref. 55.

In addition to annihilation photons, the positron beam interacting in the beryllium target also produces a continuous spectrum of bremsstrahlung photons. The bremsstrahlung-induced component of the photoneutron yield is measured independently by repeating runs at a given energy with electrons rather than with positrons. For these electron runs the field of the magnets are reversed, and beam currents comparable to those obtained with positrons are used.

The photon beam was collimated by a series of three 9.53-mm diam nickel collimators (having a total thickness of 34.3 cm), which were aligned optically. The collimation employed in these measurements differs from that of previous photoneutron measurements at Livermore; the more restricted collimation described here was made necessary by the long and narrow construction of the gas sample holders. This narrow collimation was very helpful, however, since it resulted in much tighter control of the beam tuning and hence less systematic uncertainty from this cause.

A new cylindrical, thin-walled, xenon-filled transmission ionization chamber was used to monitor the photon-beam flux. During the course of the experiment, the stability and relative response of this ionization chamber were checked periodically by placing a ^{60}Co γ-ray source into a nearby standard position. The background from cosmic rays and electronic noise was determined in separate measurements done at nearly the same time as the stability and response checks. The ion chamber exhibited no rapid drifts or erratic behavior of any kind during the course of this experiment.

The calibration of the response of the flux monitor to annihilation photons produced at the target q/a was checked at 12.3 and 22.3 MeV by observing the annihilation photons directly with a 20.32 cm by 20.32 cm NaI(Tl) photon spectrometer. This absolute photon-flux calibration was found to agree with the previous calibration. The systematic uncertainty in the photon-flux calibration is no greater than 3% at 12 MeV, but rises approximately linearly with energy to about 5% at 22 MeV.

The energy-dependent ratio k (the response of the ionization chamber to the electron-bremsstrahlung beam divided by its response to the positron-bremsstrahlung plus annihilation-photon beam) was checked at 16 different energies during this experiment, and also was found to agree with the previous calibration. The scatter in these measurements was no more than 1.5% in the energy region from 20 to 30 MeV. In order to perform this check, the current generated by the photon beam in the ionization chamber was compared to the current generated by the electron or positron beam in a secondary emission monitor connected to the annihilation target.

B. The neutron detector

The neutron detector, which nearly surrounded the samples during the measurements, consists of a 61-cm cube of paraffin in which 48 high-pressure BF_3 tubes are embedded, in four concentric rings of twelve tubes each. The neutron-yield rate from which the cross sections were calculated was derived using the number of counts registered during a gate, which began 4.5 μsec after the beam pulse and remained open for 300 μsec. The absolute efficiency at the center of the neutron detector was checked before and after the experimental runs for each sample with a Pu-Be neutron source, and the stability of the neutron detector was monitored during the experiment (about three times each day) with an Am-Be neutron source. No significant drift or erratic behavior was observed. A more detailed description of the neutron detector can be found in Refs. 54–57.

The central neutron-detector efficiencies ϵ and ϵ^2 are plotted in Fig. 2(a) as a function of neutron energy. These efficiencies are used, respectively, for reactions emitting one and two neutrons. The quantity ϵ^2 is not obtained by simply squaring the quantity ϵ, but rather contains factors, correcting for the response of the neutron detector as a function of position and for the angular distribution of the neutrons, which depend on whether a one- or two-neutron reaction is observed. Even though the energy dependence of the efficiency at the center of the detector [the top curve in Fig. 2(a)] is well known,[54–57] it was rechecked with Monte Carlo calculations (see Ref. 58). These calculations extend up to 14 MeV, where a measurement had been made previously with a d-t neutron source; this neu-

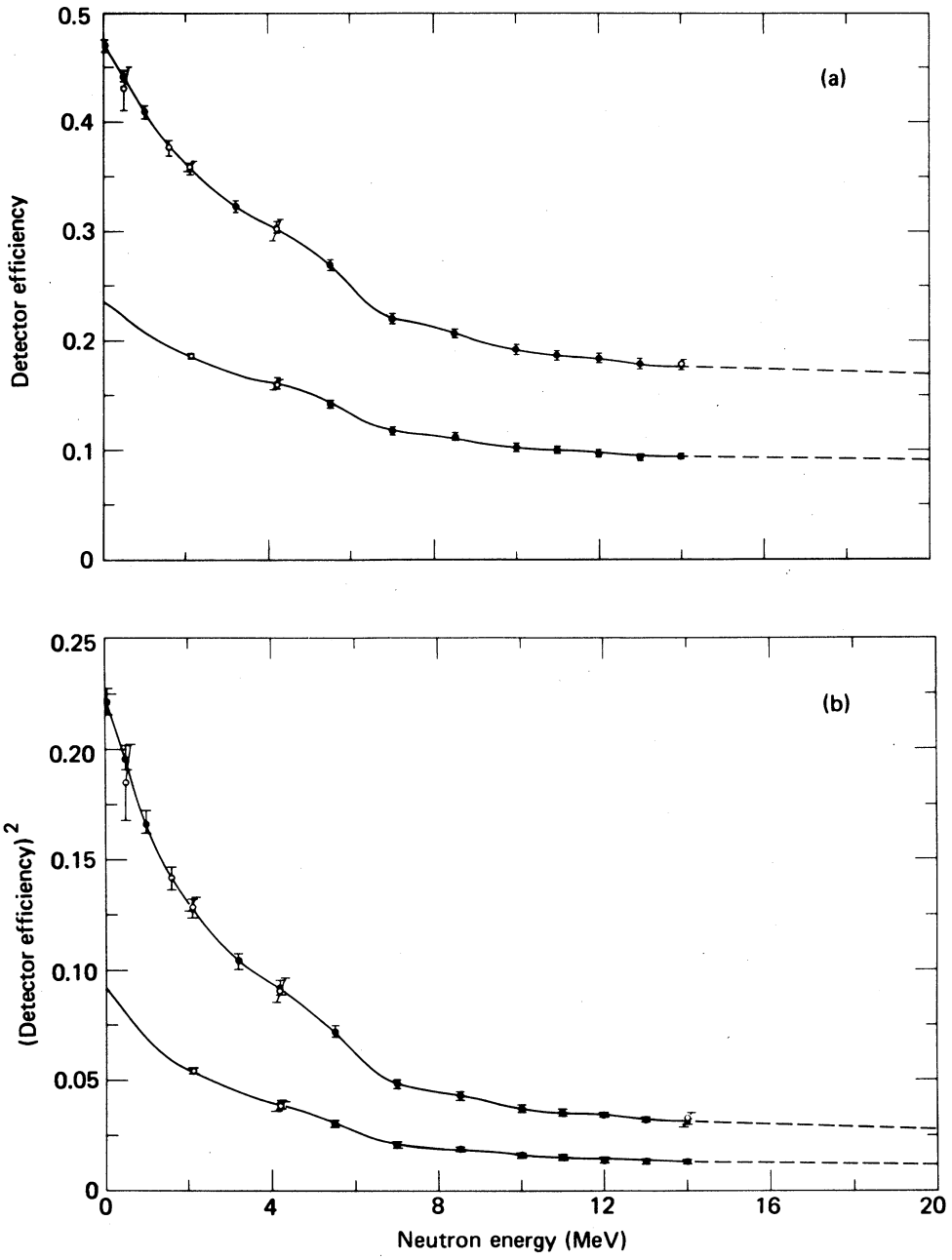

FIG. 2. (a) Neutron detector efficiency, plotted as a function of neutron energy. The open circles represent experimental measurements; the filled circles, Monte Carlo calculations. The curve fitted to the upper points is used as the efficiency for a sample located at the center of the 4π detector and from which neutrons are emitted isotropically; the lower curve is used as the efficiency for a sample distributed along the photon beam line through the detector and emitting neutrons with a $\sin^2\theta$ distribution measured with respect to the photon-beam direction. Extrapolations to neutron energies above 14 MeV are shown as dashed curves. (b) Same as in part (a) except for reactions which emit neutrons in pairs.

tron energy corresponds to a photon energy of 27.3 MeV for the reaction $^3\mathrm{H}(\gamma,n)^2\mathrm{H}$. The smooth extrapolations of the neutron-detector efficiency above 14 MeV shown in Fig. 2 were not needed for the present measurements. The falling off of the efficiency curve near 6 MeV results mainly from a maximum in the $^{12}\mathrm{C}(n,\alpha)$ reaction,[59] which acts as a sink of neutrons. Additional Monte Carlo calcula-

tions for neutron energies near 6 MeV confirm this quantitatively.

Unlike the compact liquid or solid samples used in many previous photoneutron experiments at Livermore, the gas samples which were employed in this investigation extended along the beam line beyond the fore and aft edges of the neutron detector. Therefore, the detector efficiency was measured (for neutrons having an average energy of 2.1 and 4.2 MeV) with standard ^{252}Cf and Pu-Be neutron sources as a function of position along the length of the sample. From these measurements of f, the factor $\langle f \rangle$, which multiplies ϵ to yield the effective efficiency for the distributed samples, is obtained. [For the ^{3}H(γ,2n) reaction, the factor $\langle f^2 \rangle$ (and not $\langle f \rangle^2$) converts ϵ^2 into the effective efficiency needed.] Monte Carlo calculations of this function also were performed to verify the source measurements and to show that there is no strong dependence of $\langle f \rangle$ or $\langle f^2 \rangle$ upon neutron energy. In fact, above 4.2 MeV these functions are flat and equal to 0.533 and 0.422, while at 2.1 MeV they are equal to 0.519 and 0.417; therefore, below 4.2 MeV, straightline fits were used, which yield zero-energy values of 0.504 for $\langle f \rangle$ and 0.411 for $\langle f^2 \rangle$. The effective efficiencies $\epsilon\langle f \rangle$ and $\epsilon^2\langle f^2 \rangle$ for reactions which emit single and double neutrons are shown as the lower curves in Figs. 2(a) and 2(b). Additional Monte Carlo calculations were performed in order to ascertain the effect of the $\sin^2\theta$ (rather than isotropic) photoneutron distribution which is a characteristic of all the reactions which were investigated here (θ is measured with respect to the beam direction). The resulting correction factors. 1.01 for $\langle f \rangle$ and 1.02 for $\langle f^2 \rangle$, are included in the values given above and in the lower curves of Figs. 2(a) and 2(b). Additional Monte Carlo calculations show that the presence of ^{3}H, ^{3}He, or ^{4}He gas in the sample container does not affect the detector efficiency (or $\langle f \rangle$ and $\langle f^2 \rangle$). The uncertainty in the neutron-detector efficiency for single-neutron events is about 5% for 14-MeV neutrons but shrinks to about 3% for 2-MeV neutrons; for double-neutron events it is about 7% for 14-MeV neutrons and 4% for 2-MeV neutrons. It should be noted, however, that there was no need to use the efficiency curve $\epsilon^2\langle f^2 \rangle$ above 7 MeV.

C. Samples

After passing through the ionization chamber, the collimated photon beam is incident upon the sample (and its container). Aside from the ^{3}H and ^{3}He samples, which were gases, several other samples were employed in this experiment: (a) measurements were made using oxygen, both in the form of gas and in the form of water, in order to determine the number of atoms of the sample that were irradiated by the photon beam; (b) a measurement was made using deuterium gas in order to check the scale of the absolute cross sections; (c) measurements were made of the neutron-yield rate from the empty sample containers (sample blanks) for the gases and the water sample; and (d) a measurement was made below the ^{12}C(γ,n) threshold using a 10.2-cm long polyethylene (CH_2) sample, in order to determine the number of neutrons which scatter from a sample into the neutron detector after being produced upstream of the sample. The water sample was held within a thin-walled Lucite cylinder 38 mm in diameter and 24 mm in length. The gas samples, each with a volume of about 0.5 l, were contained within cylindrical stainless-steel tubes 1 m in length and 2.54 cm in inside diameter with welded end caps which had a window thickness of 0.76 mm. These gas cells were designed for a previous experiment at Livermore.[60] The gas samples were contained at pressures such that about six atom-moles of gas were used for each measurement (for the radioactive ^{3}H sample, this amounted to 200 000 Ci). As determined by measurements with a mass spectrometer, the ^{3}H gas contained 0.5% $^2H_2$, 0.3% H_2, and $\simeq$0.3% ^{3}He, and the ^{3}He gas contained $<$0.01% ^{4}He and hydrogen isotropes. The cross-section data obtained from measurements on these samples were not corrected for these impurities; the error which results from neglecting this correction is much less than the statistical uncertainty. The masses of the samples were measured gravimetrically and, for the case of the ^{3}H-gas sample, calorimetrically as well. The uncertainty in the mass measurements was less than $\pm$0.5%. The volumes of each of the three gas pressure vessels were determined by filling them with argon gas at low pressure and then opening them to an evacuated, known volume. Once equilibrium was reached, the pressure of the system was measured, and the volume of the pressure vessel was determined using the ideal gas law. The absolute uncertainty in this volume determination was $\pm$1%, but the precision of the measurement was much better. A summary of the sample specifications is given in Table I.

In order to reduce the hazards of explosion, fire, and exposure to radioactivity, each gas-sample container (in turn) was mounted inside a secondary-containment vessel, which was a large, evacuated stainless-steel tank with 0.51-mm thick windows.

TABLE I. Sample specifications.

Nucleus	Sample mass (g)	Isotope moles	Form and pressure (MPa)[a]
^{16}O	27.01	1.50	H_2O liquid
^{16}O	96.35	6.02	O_2 gas 14.08
^{2}H	11.84	5.88	$^2H_2$ gas 15.92
^{3}He	16.89	5.60	He gas 31.36
^{3}H	18.78	6.22	$^3H_2$ gas 16.92

[a]1 MPa = 9.87 atm.

This vessel was large enough to hold all of the gas from any sample at less than atmospheric pressure. Before a measurement, this secondary-containment vessel was moved into place inside the neutron detector (and its associated shielding), and its alignment was checked *in situ* with the aid of x-ray photographs which were made with the primary electron beam from the LINAC.

The hazards associated with the gas samples employed in this investigation required extensive safety precautions in addition to the secondary containment. Details of these procedures are given in Ref. 61.

In order to determine the effective number of atoms in the gas samples intercepting the photon beam, three measurements using oxygen were made. The first was a new measurement of the absolute $^{16}O(\gamma,n)$ cross section done in the usual way[55] using a water sample. The results of this measurement[62] were found to agree very well with previous Livermore data[63] (except for a 200-keV energy shift). Next, the results of another water-sample oxygen measurement, which was performed under the same (narrow) collimation condition as was used with the gas samples, were normalized to these results; this determined the number of atoms in the beam (at the center of the neutron detector) for this collimation condition. Third, the results of a measurement using a high-pressure sample of oxygen gas were normalized to the water-sample data; this determined the effective number of atoms in the oxygen-gas sample intercepting the photon beam. The uncertainty in the measurement of the effective number of ^{16}O-gas atoms in the beam is estimated to be no larger than 2%, including the uncertainty from the water-sample measurement. Finally, the effective number of atoms in each of the other gas samples (^{3}H and ^{3}He) was computed from the ratio of the number of atom-moles of each to the number of atom-moles comprising the ^{16}O-gas sample. It should be emphasized that this procedure does not depend upon a knowledge of the $^{16}O(\gamma,n)$ cross section. Also, because these oxygen data were taken over a significant range of photon (and neutron) energies, they serve to check that no strong energy-dependent systematic error was present.

Another (but less stringent) check on the overall absolute normalization is provided by the ^{2}H data; these data agree, within the (rather large) statistical experimental limits, with the Mainz total photon-absorption data[64] and the theoretical cross-section results of Breit.[65] Both the oxygen and deuterium data discussed here are shown graphically in Ref. 66.

D. Backgrounds

The neutron yield from annihilation photons irradiating the sample is contaminated by neutrons from several other sources in addition to the background induced by positron bremsstrahlung. This beam-off background was measured often during the experiment, and, while small fluctuations were observed, they were insignificant.

Neutrons also are produced when the positron or electron beam strikes the bottom of the dump hole or the annihilation target or when the photon beam strikes the collimators or the window of the beam pipe. Although the effect of neutrons originating upstream from the sample and then scattering from the sample into the neutron detector was determined to be negligible in the measurement with the polyethylene sample, there remained a significant neutron background. With the annihilation target rotated out of the electron or positron beam, this beam-on background was measured both before and after the data run for each energy was performed. The neutron-yield rate found in this manner varied from nearly zero at the lowest energies to four times the magnitude of the machine-off background at the highest positron energies.

Finally, neutrons were produced when the photon beam encountered the tube containing a gas sample or the secondary containment vessel (particularly their end windows). The neutron yield from the sample blank was determined in a separate measurement performed with the same apparatus as that which was used for the gas measurement. Variation of the alignment of the sample tube within the secondary-containment vessel resulted in a somewhat different normalization m of the net sample-blank neutron-yield rate for each gas sample mea-

sured (see below). The neutron-yield rate for the water-sample blank was measured sequentially, for each energy, with the neutron-yield rate from the water sample itself, with the aid of a remotely controlled sample changer.

III. DATA ANALYSIS AND EXPERIMENTAL UNCERTAINTIES

The data-analysis procedures for this experiment were largely the same as have been developed and used for several other recent photonuclear measurements at Livermore.[55,62,67] The data were reduced to cross sections in several discrete steps. Corrections to the data were made first for pileup effects and then for the drifts of the flux monitor and the neutron detector. The background contaminating the counts from the flux monitor q and the counts from the neutron detector n were subtracted, and neutron-yield rates n/q were computed. The neutron-yield rates from runs which were performed with incident electrons were multiplied by the normalizing factor k in order to determine that part of the neutron-yield rate for each sample resulting from positron bremsstrahlung. After the positron-bremsstrahlung yield rates were obtained in this manner, they were fitted and subtracted from the total neutron-yield rates from positron runs. Yield rates from the sample-blank runs were subtracted next, and all the resulting net neutron-yield rates except that for the reaction $^3H(\gamma,n)$ were ready for conversion into cross sections. [A further correction to the net n/q data for this reaction was required to account for the contamination of neutrons from $^3H(\gamma,2n)$ reactions (the multiplicity correction).]

A. Pileup correction

Since the photoneutron cross sections for both ^3H and ^3He are small, and since the samples were gases, the counting rates, even at the maximum attainable beam currents, were too low to make pileup significant; even above 24 MeV, the pileup constituted at most 15% of the double-neutron detections arising from true $^3H(\gamma,2n)$ events. The uncertainty resulting from this source is less than 1%.

B. Subtraction of backgrounds

After correcting the data for the drift of the flux monitor, background counts which were induced by the beam, cosmic rays, and electronic noise were subtracted both from the flux-monitor data and from the neutron-detector data for all the samples. The background counts recorded by the flux monitor result primarily from stray ionization and from electronic noise. Since each such count represents an accumulation of a very large number of small pulses, the number of counts recorded by the flux monitor during a single beam-on background run is an accurate measure of the flux-monitor background for that beam energy and polarity.

On the other hand, the background counts recorded by the neutron detector are single-event phenomena, caused chiefly by real neutrons. The single-neutron counts which were measured during the beam-on background runs ranged from almost 100% of the foreground near the $^3H(\gamma,n)$ and $^3He(\gamma,n)$ reaction thresholds to less than 1% of the foreground at the highest beam energies employed. Because of the requirement of the 300-μsec coincidence gate, however, the double-neutron background contaminating the $^3H(\gamma,2n)$ data was negligible.

Moreover, since runs at the same energies or at nearby energies yielded, within the rather poor statistics of a single run, nearly the same values for the beam-on neutron background, and since at low energies, where the neutron background was largest relative to the foreground, the average rate for counting neutrons with the annihilation target removed and the beam on was equal to the average rate for counting neutrons with the beam off, the contribution of the single-event neutron background to the overall statistical uncertainty also is negligible.

C. Subtraction of the neutron yield from bremsstrahlung

After subtracting the background of neutrons which did not originate from the sample or sample blank, the neutron-yield rate from photoneutrons produced by bremsstrahlung, as determined from the runs with electrons, was subtracted (after multiplication by the energy-dependent factor k). The systematic uncertainty (about 1.5%) in determining k was not included in the statistical uncertainties calculated for the cross-section data points. The single-neutron yield rates which have been corrected for pileup and background contamination are shown in Fig. 3. Similarly, the double-neutron yield rates are shown in Fig. 4. The electron-bremsstrahlung yield rates shown in these figures were fitted with

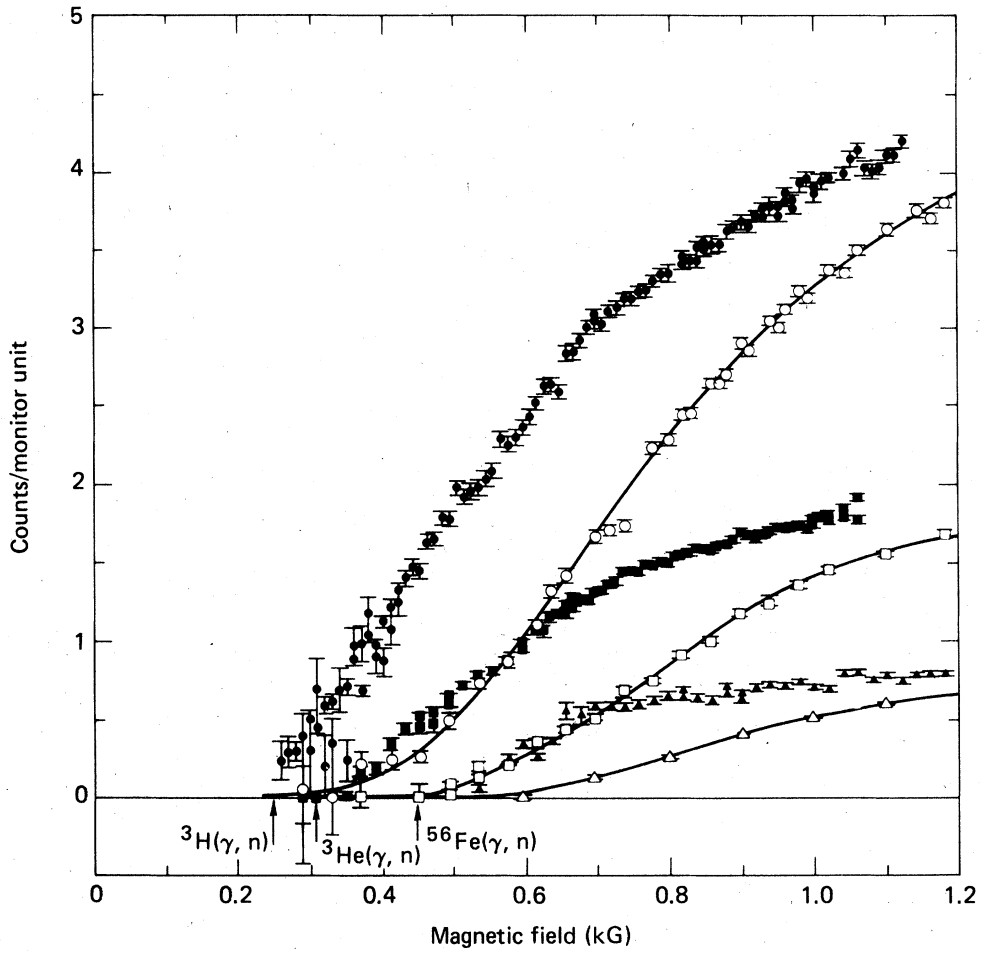

FIG. 3. Single-photoneutron yield rates for ^{3}H runs (circles), ^{3}He runs (squares), and sample-blank runs (triangles), as a function of the magnetic field of the energy-analyzing magnet (1 kG corresponds to 24.8 MeV). The upper points for each sample (filled symbols) are for incident positrons, and the lower points (open symbols) are for incident electrons. The curves, which are fitted to the incident-electron data, were used for subtraction of the photoneutron yield resulting from positron bremsstrahlung. The (γ,n) reaction thresholds for ^{3}H, ^{3}He, and the ^{56}Fe component of the stainless steel sample blank are indicated by the arrows.

the smooth, monotonically increasing curves (also shown in these figures) used for subtracting the neutron yield resulting from positron bremsstrahlung. The statistical uncertainties for the positron-run data points are so much larger than the fitting uncertainties for these curves that the latter are ignored in the computation of the error flags for the cross-section data points. The annihilation-photon yield rates (after the bremsstrahlung-yield subtractions) for single-neutron events and double-neutron events are shown, respectively, in Figs. 5 and 6.

D. Subtraction of the neutron yield from the sample blank

At this point, the net sample-blank yield rates were subtracted from the net sample-in yield rates. Smooth curves were fitted before subtraction to the single- and double-neutron sample-blank yield rates; these curves are shown, respectively, in Figs. 5 and 7. Smooth representations of the sample-blank data were used in order to reflect the expected shapes of the photoneutron cross sections for iron.

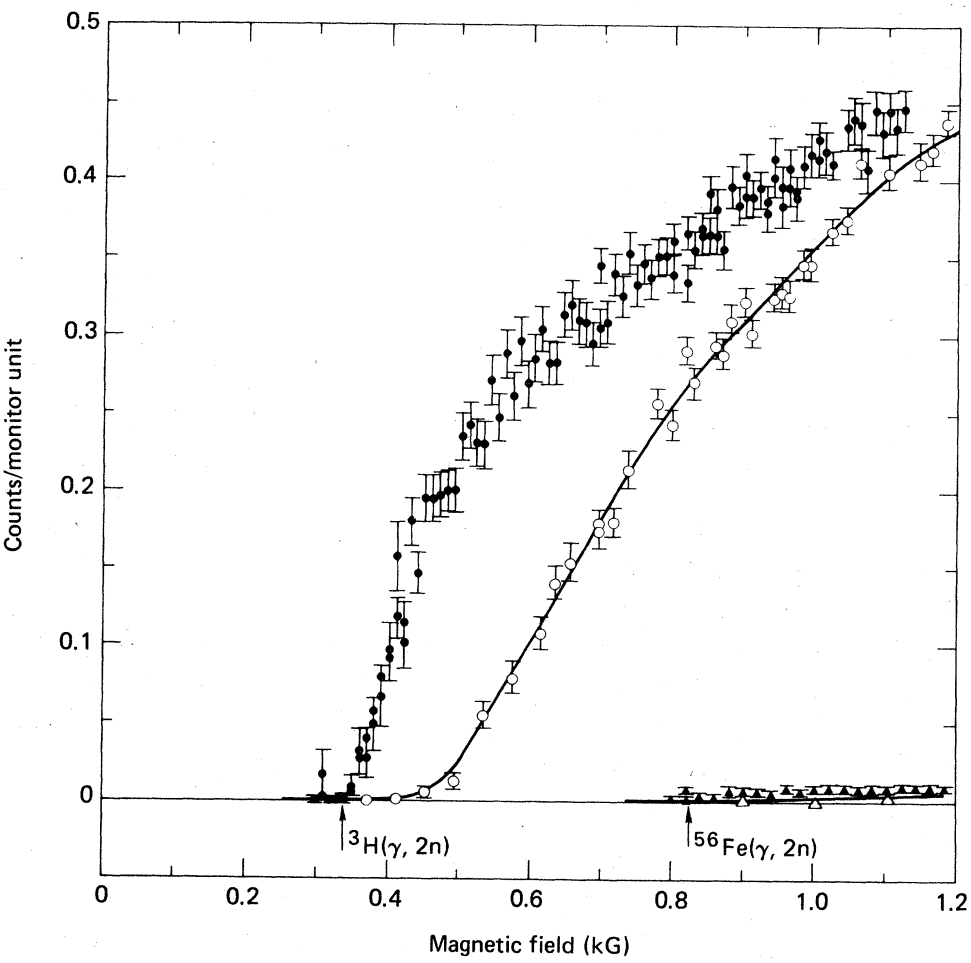

FIG. 4. Double-photoneutron yield rate for ^{3}H runs (circles) and sample-blank runs (triangles), as a function of the magnetic field of the energy-analyzing magnet (1 kG corresponds to 24.8 MeV). The upper points for each sample (filled symbols) are for incident positrons, and the lower points (open symbols) are for incident electrons. The curves, which are fitted to the incident-electron data, were used for subtraction of the photoneutron yield rate resulting from positron bremsstrahlung. The $(\gamma,2n)$ reaction thresholds for ^{3}H and the ^{56}Fe component of the stainless steel sample blank are indicated by the arrows.

In order to determine the normalizing constant m for the ^{3}He-gas sample, the double-neutron yield rates for that sample [all such events in ^{3}He are the result of $(\gamma,2n)$ reactions in the stainless-steel containment vessels] and the sample blank (shown in Fig. 7) were integrated over energy (up to 26.3 MeV). A comparison of the two integrated yield rates resulted in a value of m for ^{3}He of 0.83 $\pm$ 0.03. More qualitative evidence helped to determine the value of m for the case of the ^{3}H-gas sample. This evidence was obtained by comparing the structure of the single-neutron sample-blank yield rate with the structure of the single-neutron yield rate of the ^{3}H-gas sample and also by comparing the x-ray photographs taken after completing the alignment of the gas-sample tubes and the sample-blank tube. First, m was treated as a statistical quantity which was the average of the values of m for the sample blank (1.0), ^{3}He (0.83), and a measurement[66] of the reaction ^{4}He(γ,n) (0.96); then, after consideration of the qualitative evidence, this number was reduced to 0.88. The systematic uncertainty in m for ^{3}H, which mainly affects the accuracy of the absolute scale of the measured (γ,n) cross section, for which the sample-blank background was relatively large, is no more than 5%. The net

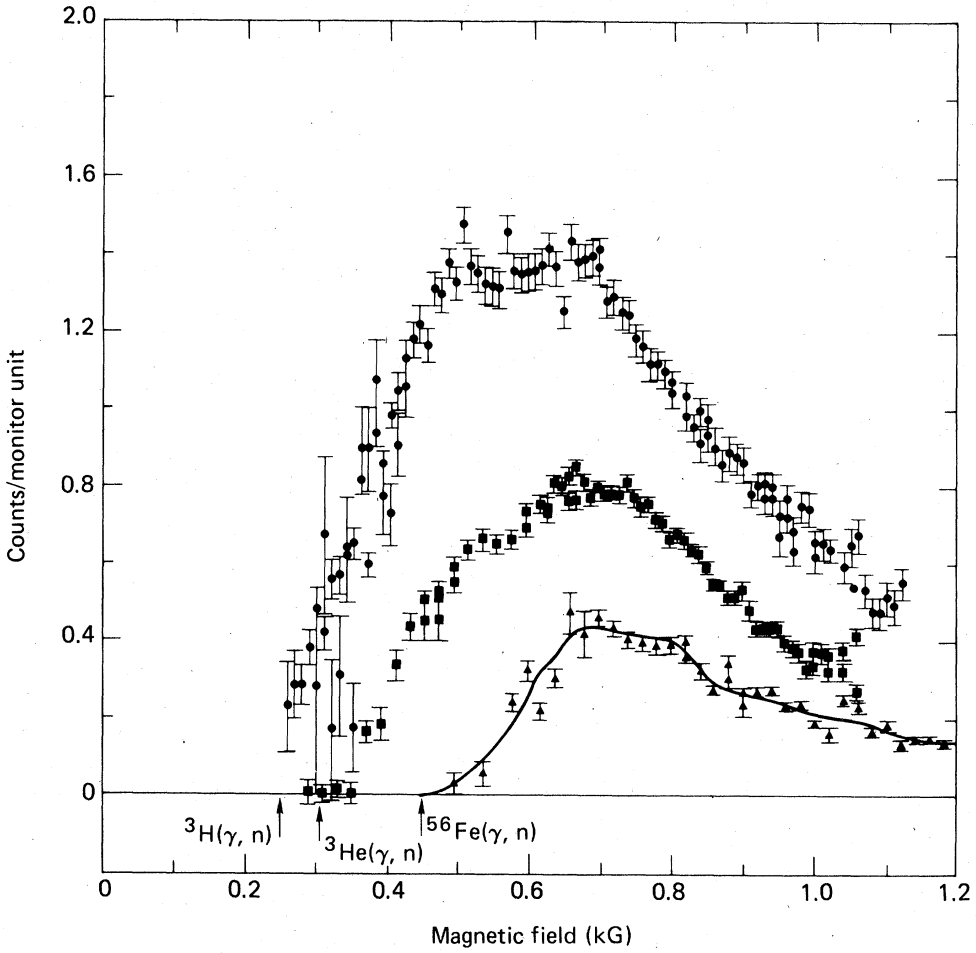

FIG. 5. Single-photoneutron yield rate for ^{3}H runs (circles), ^{3}He runs (squares), and sample-blank runs (triangles) after subtraction of the yield rate from positron bremsstrahlung. The curve, which is fitted to the sample-blank data, was used for the subtraction of the sample-blank yield rate from the sample-in yield rates. The principal source of the sample-blank yield rate was the ^{56}Fe(γ,n) reaction on the steel windows; the sample-blank curve is seen to resemble the (γ,n) cross section for a nucleus like ^{56}Fe (see, for example, Ref. 67).

single-neutron yield rates for ^{3}H and ^{3}He are compared in Fig. 8 [the data for ^{3}H are not yet corrected for neutrons from the ^{3}H(γ,2n) reaction]. The estimated uncertainty in fitting the sample-blank yield rate is included in the error flags of Fig. 8, but the (systematic) uncertainty in m is not.

E. Neutron-detector efficiency and multiplicity correction

Once the sample-blank yield rates were subtracted from the sample-in data, the ^{3}H-gas single-neutron-event data were ready for the multiplicity correction. To make this correction the efficiency of the neutron detector must be known as a function of incident photon energy and of event multiplicity.[55] For the present measurements with the long gas-sample tubes, a new calibration of the efficiency was required, which, as described above, gives $\epsilon\langle f\rangle$ and $\epsilon^2\langle f^2\rangle$ as functions of the neutron energy (Fig. 2).

The average neutron energies for the various photoneutron reactions measured here also must be known as a function of photon energy in order to make use of the curves of Fig. 2. Fortunately, for the reactions ^{3}H(γ,n) and ^{2}H(γ,n), the neutron energy is established uniquely by the two-body kinematics; for ^{16}O(γ,n), the neutron energies had been measured previously.[56] However, for the three-body

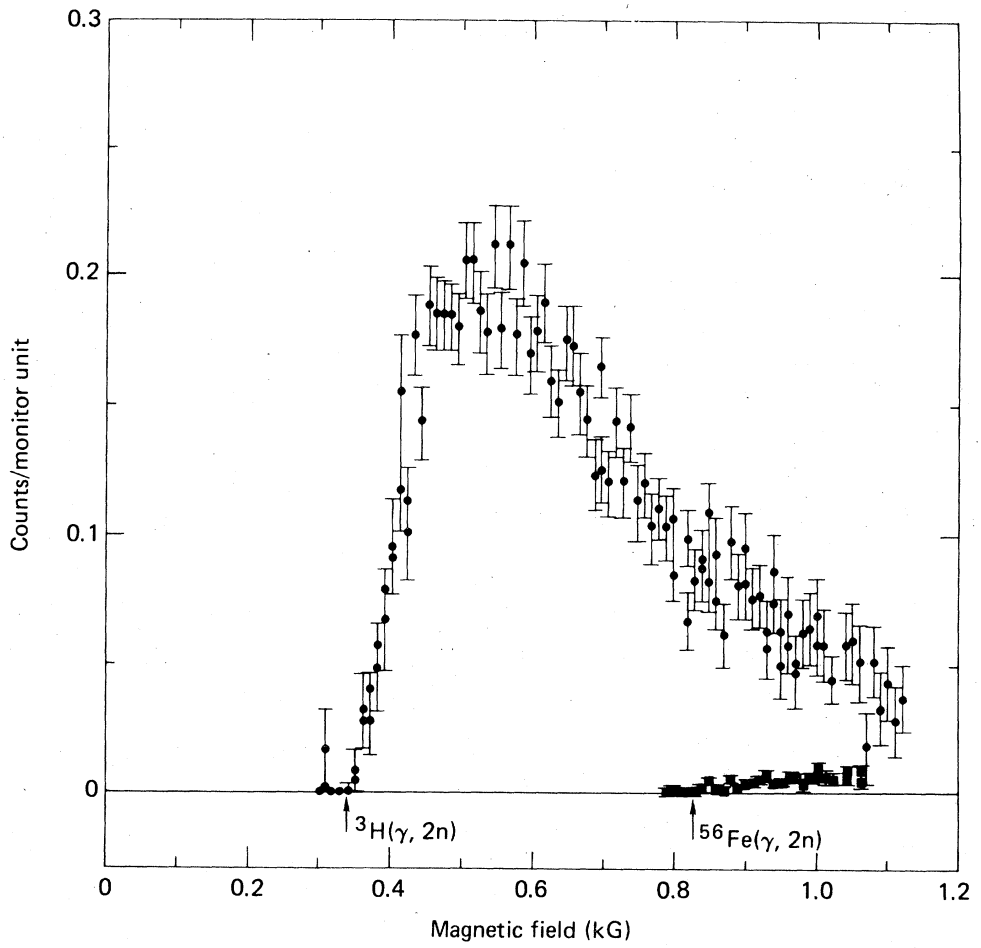

FIG. 6. Double-photoneutron yield rate for ^{3}H runs (circles) and ^{3}He runs (squares) after subtraction of the yield rate from positron bremsstrahlung. The (small) double-photoneutron yield rate recorded for the ^{3}He runs comes chiefly from $(\gamma,2n)$ reactions in the windows of the gas cell and of the secondary-containment vessel.

breakup reactions of ^{3}H and ^{3}He the final-state energy distributions of the photoneutrons are needed. These distributions were obtained from the (Faddeev-model) calculations of Gibson and Lehman.[68] The distribution for ^{3}He, when corrected for the Coulomb repulsion between the protons (see Ref. 48), is in good agreement with the fragmentary experimental evidence of Gorbunov *et al.*[12] and of Hendry and Macleod.[69] (Cloud chambers were used in both of these experiments.) By folding together these neutron-energy distributions with the efficiency curves for either $\epsilon\langle f\rangle$ or $\epsilon^2\langle f^2\rangle$, average efficiencies $\langle\epsilon\rangle$ or $\langle\epsilon^2\rangle$ for the two reactions leading to a three-body final state were obtained as a function of the photon energy. The accuracy of this method is justified not only by our confidence in the calculations of Ref. 68, but also by the insensitivity of the average detector efficiency to changes in these shapes (see Fig. 2). Thus, it turns out that the systematic uncertainty in the average detector efficiency for ^{3}H$(\gamma,2n)$ and ^{3}He(γ,n) which is attributable to the theoretically derived shapes for the neutron-energy distributions is less than 1%.

F. Systematic uncertainties

Compariable contributions to the systematic uncertainty in the cross sections come from the uncertainties of all of the multiplicative factors (except that for g, which is negligible) which convert the raw neutron-yield rates into cross sections [see Eqs. (1) and (2)]. The systematic uncertainty for each of these factors is given in Table II. At 22 MeV the

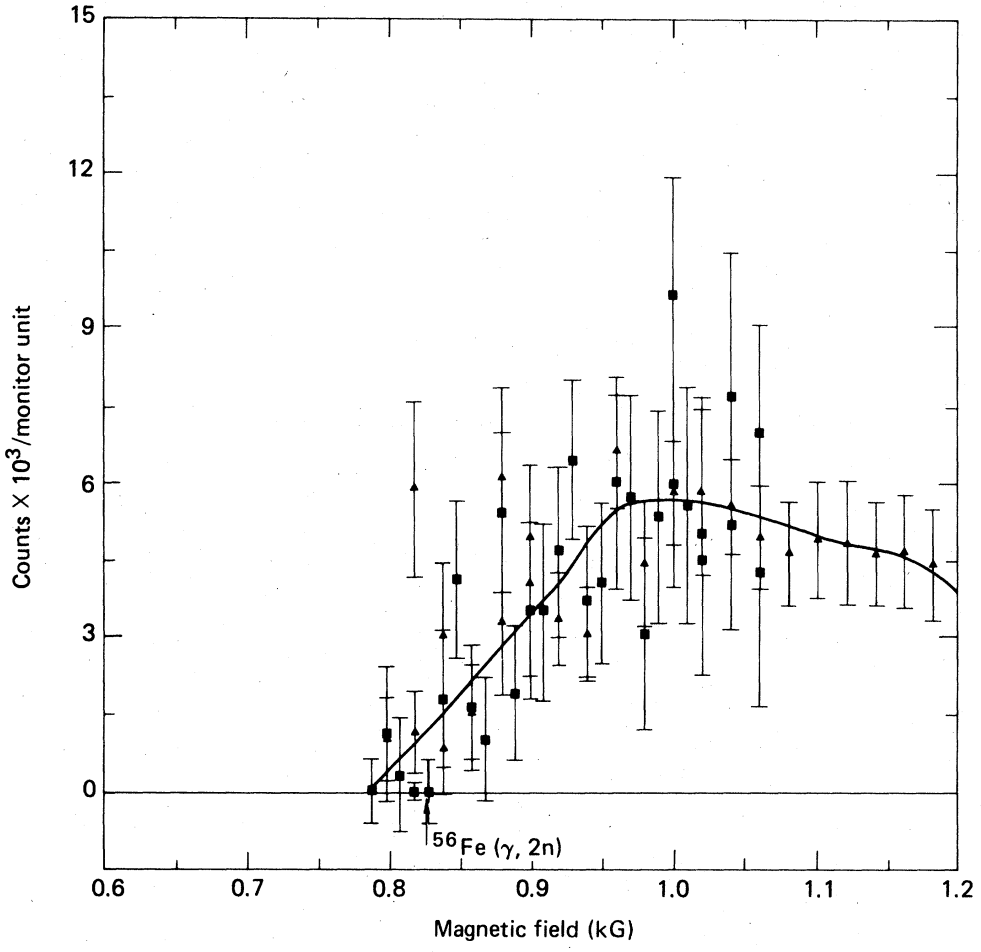

FIG. 7. Double-photoneutron yield rate for ^{3}He runs (squares) and sample-blank runs (triangles) after subtraction of the yield rates from positron bremsstrahlung. The curve, which was fitted to the sample-blank data, was used for the subtraction of the sample-blank yield rate from the sample-in yield rates. The principal source of the sample-blank yield rate was the ^{56}Fe(γ,2n) reaction on the steel windows; the sample-blank curve is seen to resemble the (γ,2n) cross section for a nucleus such as ^{56}Fe (see, for example, Ref. 67).

contribution from the uncertainty in m is $\sim 1.5\%$ for the ^{3}H(γ,n) cross section and $\sim 3\%$ for the ^{3}He(γ,n) cross section, but contributes very little to the systematic uncertainty of the ^{3}H(γ,2n) cross section. The overall systematic uncertainty for all three of the measured cross sections is estimated to be $\sim 8\%$ at 12 MeV, $\sim 12\%$ at 22 MeV, and $\sim 15\%$ at the highest energies reported here. These systematic uncertainties are of approximately the same magnitude as the statistical uncertainties. The cross-section results reported in this paper were averaged at the same energy where data points were repeated and then averaged in wider energy bins where the statistics were relatively poorer.

IV. RESULTS AND DISCUSSION

A. Measured cross sections

The results of the present measurement of the ^{3}He(γ,n) cross section are shown as the filled circles in Fig. 9. The statistical uncertainties range from $3-5\%$ in the peak region from about 11 to 21 MeV, and then increase to $\sim 8\%$ at the highest energies.

Figure 9 shows as well the results of Gorbunov *et al.*,[12] who used bremsstrahlung incident on ^{3}He gas in a cloud chamber, the results of Gerstenberg and O'Connell,[30] who used bremsstrahlung incident

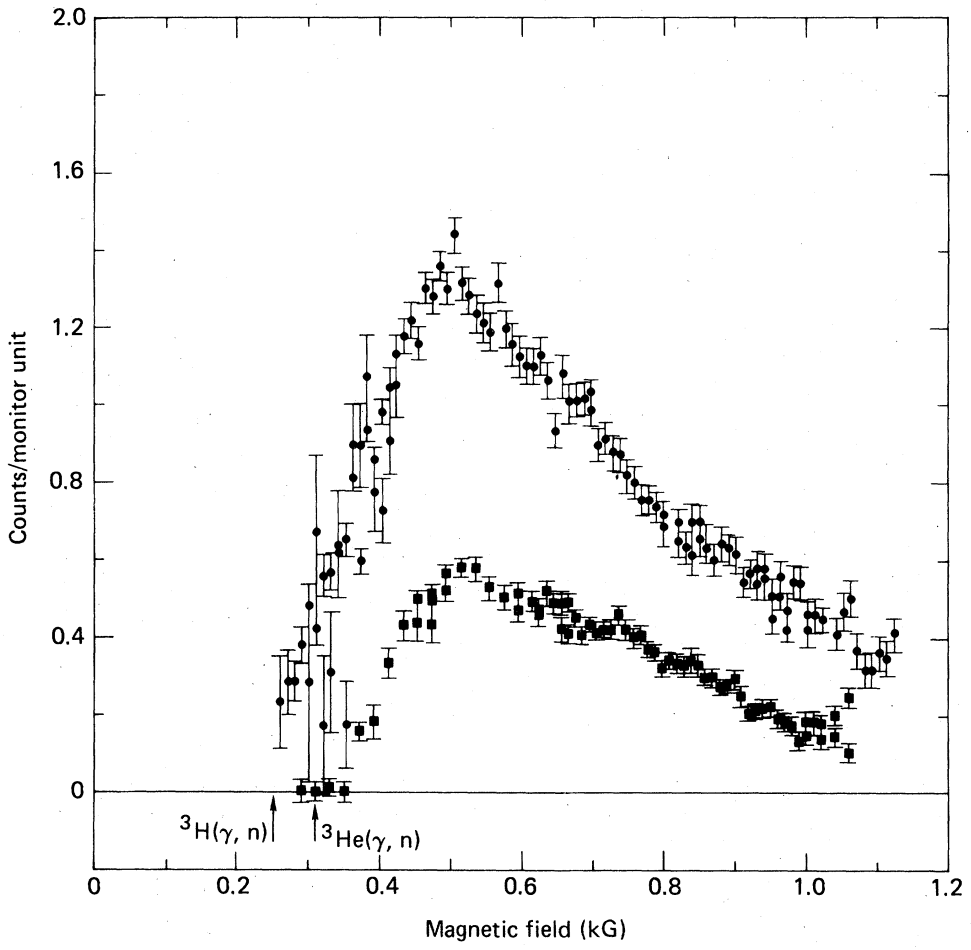

FIG. 8. Net single-photoneutron yield rates for ^{3}H runs (circles) and ^{3}He runs (squares) after subtraction of the normalized single-photoneutron sample-blank yield rates. The ^{3}H data have not yet been corrected for contamination by neutrons from the ^{3}H(γ,2n) reaction (the multiplicity correction; see text).

on a liquid-^{3}He sample, and the results of Berman *et al.*,[31] who used monoenergetic photons incident on a liquid-^{3}He sample. The energy resolution of the annihilation-photon experiment of Ref. 31 (open circles) is better than that of the two bremsstrahlung experiments (2.5% vs 5–10%). The statistical uncertainties near the peak amount to 10% of the cross section for the data of Ref. 30 (dashed histogram) and 18% of the cross section for those of Ref. 12 (solid histogram). The results of Ref. 31 exhibit some evidence for structure in the cross section near 12 MeV and between 17 and 24 MeV. The flatness of the ^{3}He cross section just above threshold which is observed in the present measurement was foreshadowed by the results of Ref. 31 (which, however, have poorer statistics there) but cannot be seen in the data of Refs. 12 or 30. The data of this experiment agree better in the region of the steep rise below 13 MeV with the data of Ref. 12 and Ref. 31 than with the data of Ref. 30. From 13 MeV to the maximum energy of 25.8 MeV, the present results

TABLE II. Systematic uncertainties.

Factor	Uncertainty (%)	Effect on cross section (%) at 12 MeV	at 22 MeV
k	1.5	1	5
m	3.5–5	~0	0–3
q/a	3–6	3	5
saf	2.5	2.5	2.5
$\langle\epsilon\rangle$	3–5	3	4
$\langle\epsilon^2\rangle$	4–7	4	5

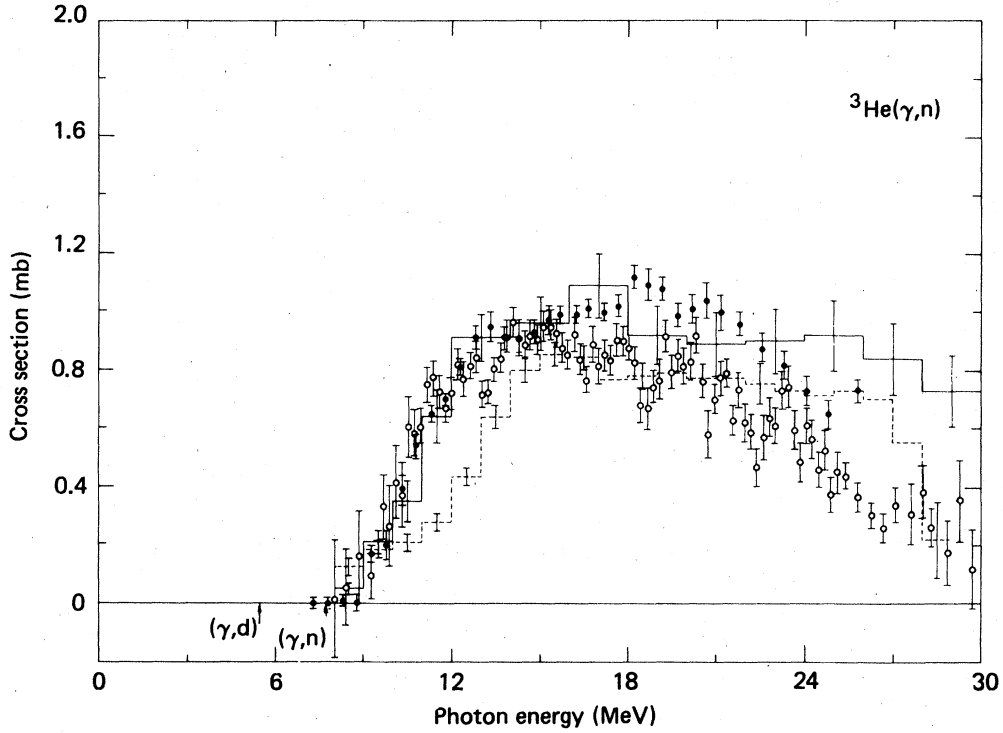

FIG. 9. Three-body photodisintegration cross section for ^{3}He: filled circles, present data; open circles, data of Ref. 31; solid histogram, Ref. 12; dashed histogram, Ref. 30. The error flags indicate statistical uncertainties only. The arrows in this and the following figures indicate the reaction thresholds, as labeled.

agree best in magnitude with the data of Ref. 12, although they lie 10% higher in the region of the peak at 18 MeV and fall faster at higher energies. The more rapid decrease of the cross-section results of Ref. 31 probably can be attributed to an incorrect extrapolation of the neutron-detector efficiency above ~ 6 MeV (neutron energy). Although there is some evidence for a weak peak at ~ 13 MeV and for some structure between 18 and 21 MeV, the results of the present measurement of ^{3}He(γ,n) only partly support the more pronounced indications of structure between 12 and 14 MeV and between 17 and 24 MeV seen in the results of Ref. 31.

The cross-section results for the present measurement of ^{3}H(γ,n) and ^{3}H(γ,2n) are shown, respectively, in Figs. 10 and 11. The statistical uncertainties for the ^{3}H(γ,n) data (Fig. 10) are relatively large, primarily because of the large multiplicity correction discussed above; they range from $5-10\%$ between about 8 and 11 MeV, and are typically $\sim 15\%$ from 11 to 16 MeV and $\sim 20-25\%$ above 16 MeV. The results of previous measurements also are shown in Fig. 10; one sees that although the present cross section near 23 MeV is considerably higher than that reported in Ref. 34 (open circles), its rise matches very well the sparser data of Ref. 33 (open squares).

The statistical uncertainties for the ^{3}H(γ,2n) data (Fig. 11) range from $5-7\%$ in the peak region from about 13 to 20 MeV, then increase gradually to $\sim 20\%$ at the highest energies. The datum at 10.8 MeV from the experiment of Bösch *et al.*[33] (the open square) is seen to be in good agreement with the present data.

B. Comparison with theory

The ^{3}He(γ,n) data of this measurement are displayed in Fig. 12(c), together with the theoretical results of Barbour and Phillips,[44] Gibson and Lehman,[48] and Fang *et al.*[52] The results of Ref. 44 were the first to be obtained for this reaction with the Faddeev treatment and an s-wave spin-dependent separable-potential model. The results of

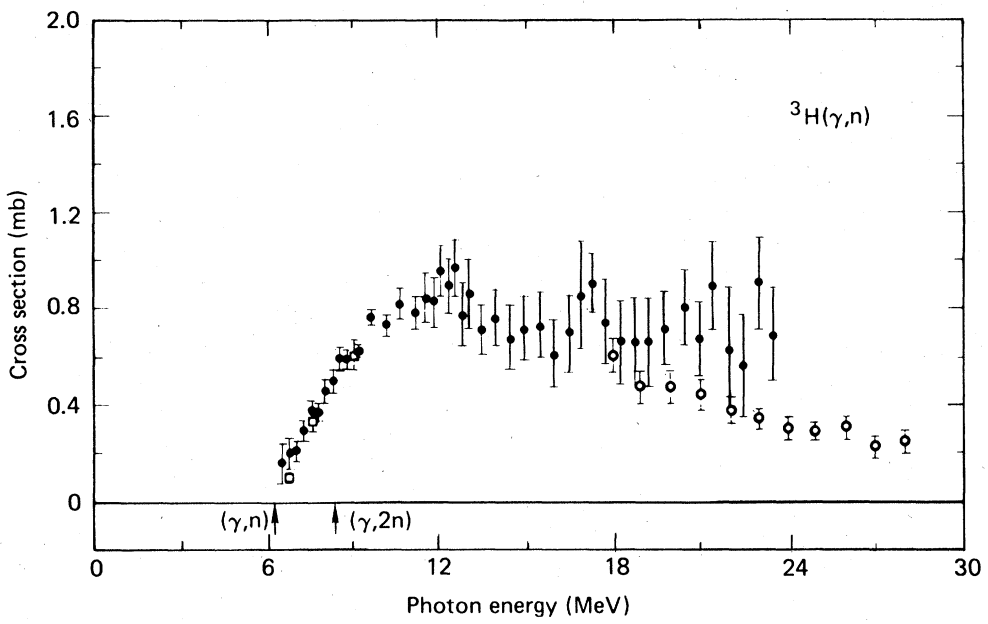

FIG. 10. Two-body photodisintegration cross section for ^{3}H: filled circles, present data; open squares, data of Ref. 33; open circles, Ref. 34. The error flags indicate statistical uncertainties only.

Ref. 48 were obtained from another Faddeev calculation of the $E1$ photodisintegration. Gibson and Lehman calculated consistently both the ground-state and final-state wave functions (Barbour and Phillips used an empirical form for the ground-state wave function, fitted to the measured trinucleon charge radii), but they neglected the S'-state contributions (which Barbour and Phillips included) and

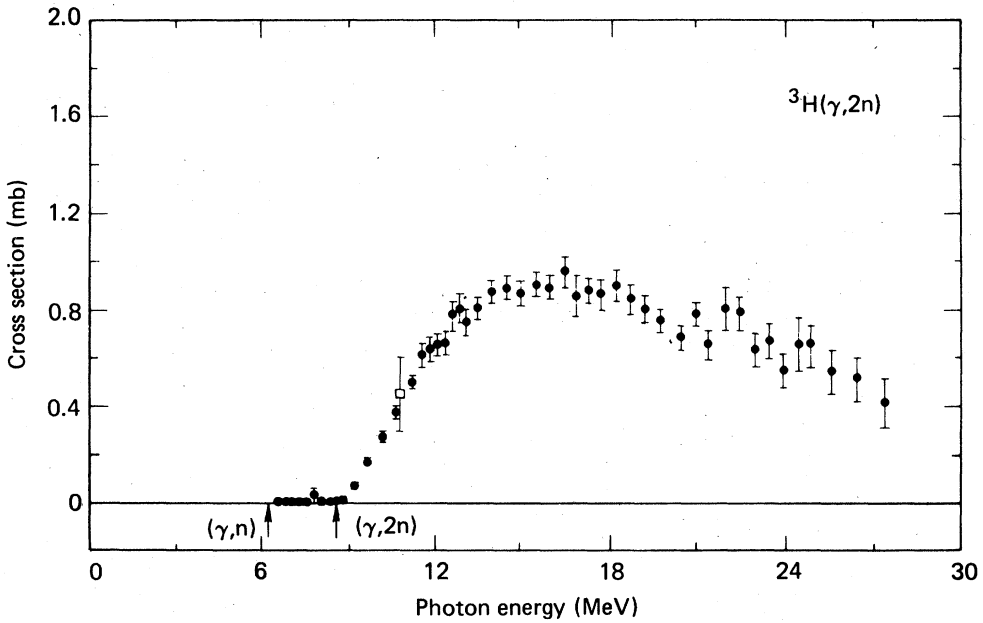

FIG. 11. Three-body photodisintegration cross section for ^{3}H: filled circles, present data; open square, datum of Ref. 33. The error flags indicate statistical uncertainties only.

the Coulomb repulsion of the two protons (which Barbour and Phillips also neglected). Both of the calculations[44,48] which use the Faddeev method give cross-section results that peak lower in energy and more sharply than the present data, although the result of Ref. 48 is a much better representation of the data than that of Ref. 44. The calculation[52] which uses an expansion in hyperspherical harmonics produces a cross section that peaks higher in energy, in better agreement with the shape of the measured cross section. This result is relevant only to the $T = \frac{3}{2}$ component of the cross section; it is not yet understood how to handle (in this formalism) the mixed boundary condition required for the simultaneous treatment of the $T = \frac{1}{2}$ coupled n-d and n-n-p channels. However, from the work on ^{3}He(γ,2p) of Barbour and Phillips or of Gibson and Lehman, it can be inferred that the final-state $T = \frac{3}{2}$ part of the ^{3}H(γ,2n) or ^{3}He(γ,n) cross section should be about 90% of the three-body breakup cross section, and therefore that the hyperspherical-harmonics results for the $T = \frac{3}{2}$ component should constitute reasonable lower limits for the three-body breakup cross sections. The results of the calculation of Ref. 48 do not extend down to the ^{3}He(γ,n) reaction threshold as do the other two; and only that of Ref. 52 produces the slow rise just above threshold which is observed for the ^{3}He(γ,n) data of this experiment. However, this behavior is probably the result of excluding the $T = \frac{1}{2}$ part of the three-body cross section.

For the three calculational results which are shown in Fig. 12(c), no combination of potential, wave functions, and method of calculation is repeated. When compared with the present data, only the results of Ref. 44 can be excluded, but none of the theoretical results is entirely acceptable. Each of the three models can be improved. For instance, as is mentioned above, the excessive peaking which is seen for the result of Barbour and Phillips can be attributed to an incorrect ground-state wave function. The inadequate magnitude of the ^{3}He(γ,n) cross section which was computed by Fang *et al.* can be attributed, in part, to the exclusion of that part of the three-body breakup which has $T = \frac{1}{2}$ in the final state. The calculation of Gibson and Lehman should compare more favorably with the data if tensor forces, an admixture of the S' state, and the Coulomb repulsion of the two protons were included in their model (see Ref. 48).

Despite the wealth of experimental data there is disagreement among the reported values of the ^{3}He(γ,d) cross section at the peak of the giant reso-

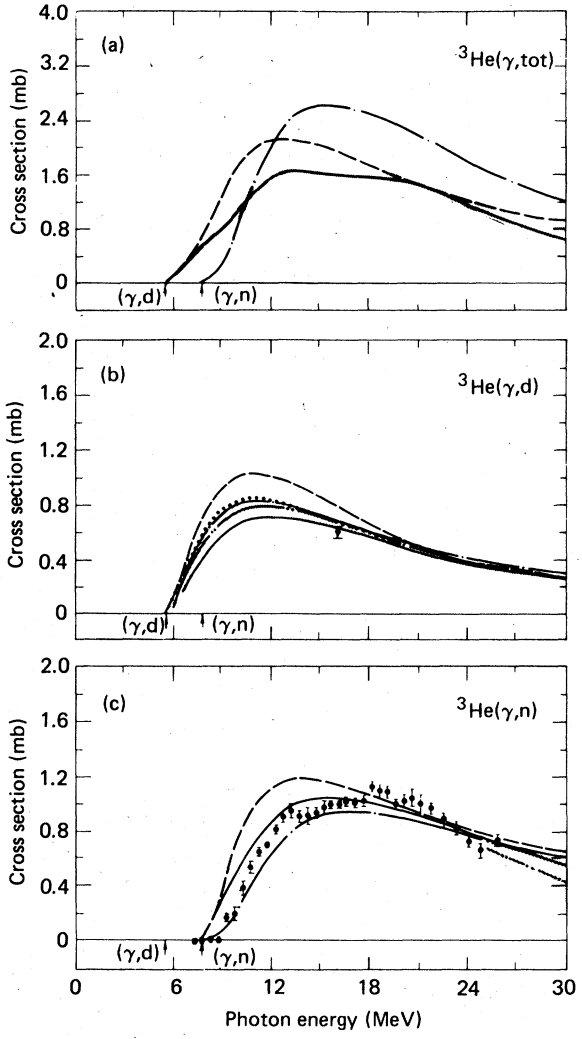

FIG. 12. (a) Total photodisintegration cross section for ^{3}He: The solid curve with shaded error band is taken from the data compiled in Ref. 17 for the ^{3}He(γ,d) cross section combined with the present data for ^{3}He(γ,n); the dashed curve is the sum of the theoretical predictions for ^{3}He(γ,d) and ^{3}He(γ,n) from Ref. 44; the dash-dot-dash curve is the theoretical prediction from Ref. 53. (b) Two-body photodisintegration cross section for ^{3}He: shaded band, data from Ref. 17; point with error flag, datum of Ref. 28; dashed curve, theoretical prediction from Ref. 44; solid curve, dash-dot-dash curve, dash-dot-dot-dash curve, and dotted curve, theoretical predictions from Ref. 72 using SSC*C*, GPDT, SSC*A*, and SSC*B* potentials, respectively (see text). (c) Three-body photodisintegration cross section for ^{3}He: filled circles, present data; dash-dot-dot-dash curve with shaded error band, extrapolation of the present data; dashed curve, theoretical prediction from Ref. 44; solid curve, theoretical prediction from Ref. 48; dash-dot-dash curve, theoretical prediction from Ref. 52.

nance (near 12 MeV).[17,29] In the vicinity of this peak the measurements fall into two discrete groups, one centered at about 0.75 mb and the other at about 0.92 mb. As discussed in Ref. 22, the electrodisintegration measurements of Refs. 19 and 21, which lie in the upper group, overestimate somewhat the ^{3}He two-body photodisintegration cross section, since for these results an incorrect virtual-photon spectrum was assumed. (However, the magnitude of this correction in the conversion of the electrodisintegration data is probably only a few percent.) The paper of Ticcioni *et al.*[17] reports the measurement of the ^{3}He(γ,d) cross section with the smallest statistical error (about 1% at the peak), and these results lie in the lower group of data; the cross section of Ref. 17 rises from the threshold at 5.49 MeV to a peak of 0.75 mb near 12 MeV and falls monotonically to a value of 0.27 mb at 30 MeV. The ^{2}H(p,^{3}He) experiment of Matthews *et al.*[28] [at $E_p = 16$ MeV, which corresponds to $E_\gamma = 16.1$ MeV in the inverse ^{3}He(γ,d) reaction] was designed expressly to determine the absolute value of the cross section; the result of this measurement agrees with that of Ticcioni *et al.*

The shaded band in Fig. 12(b) represents the experimental cross section for the two-body photodisintegration of ^{3}He. The data are taken from the lower group of points in the paper by Ticcioni *et al.*[17] These data are a combination of several different measurements at different laboratories and are in agreement with the datum, also shown in Fig. 12(b), from the experiment of Matthews *et al.*[28] These experimental data are compared with the calculations of Barbour and Phillips[44] and the unpublished results of Ballot and Fabre de la Ripelle.[70] Ballot and Fabre de la Ripelle calculated the ^{3}He(γ,d) cross section with four different potentials and a hyperspherical-harmonics formalism. The four potentials which were used, namely three Sprung-de Tourreil super-soft-core potentials (SSC*A*, SSC*B*, and SSC*C*) and a Gogny-Pires-de Tourreil super-soft-core potential (GPDT), differ from each other by the relative strength of their central, LS tensor, and L^2 components. The ground-state wave functions, which were calculated with these potentials in order to determine the ^{3}He(γ,d) cross section, include admixtures of both the S' and the D states. Good agreement with the data is obtained by all four potentials, especially the SSC*A* potential (the dash-dot-dot-dash curve). That the Barbour and Phillips result (the dashed curve), which was obtained with a separable-potential model and a Faddeev-type calculation, overestimates the cross section is primarily the result of an incorrect choice of the ground-state wave function and not the result of including an admixture of the S' state. Finally, Gibson and Lehman estimated that the effect of modifying the strong interaction to simulate the Coulomb repulsion in just the final state would be only a 1% reduction in the ^{3}He(γ,d) cross section at the peak.[47]

The solid line with shaded error band in Fig. 12(a) represents the total cross section for the photodisintegration of ^{3}He. The data for the total cross section were obtained by adding the three-body photodisintegration data of this experiment to the two-body photodisintegration data shown in Fig. 12(b). In order to extend the total cross section data to 30 MeV, the ^{3}He(γ,n) data were extrapolated as indicated by the dash-dot-dot-dash line with the shaded error band in Fig. 12(c). Two calculations are compared with the experimental results in Fig. 12(a): the theoretical result of Levinger and Fitzgibbon[53] (calculated using hyperspherical harmonics with a V^x potential) predicts more strength at the peak (about 2.6 mb) than the theoretical result of Barbour and Phillips,[44] which was constructed from their predictions for the two- and three-body breakup of ^{3}He. The discrepancy between the prediction of Ref. 53 and the data, in the energy range between the thresholds for two- and three-body breakup and at the peak of the cross section, can be attributed to the methodological problems which arise in establishing a simultaneous boundary condition for both the $T = \frac{1}{2}$ and $\frac{3}{2}$ parts of the cross section.

The present ^{3}H(γ,n) data are compared in Fig. 13(b) with the theoretical results of Rahman *et al.*,[39] Bösch *et al.*,[33] and Gibson and Lehman [obtained by multiplying the 90° differential cross section of Ref. 47 by $8\pi/3$ (assuming a $\sin^2\theta$ distribution)]. None of the theoretical results in Fig. 13(b) can be excluded by the present data alone; however, the addition of a tensor force to the separable-potential Faddeev calculation (solid curve) should improve the agreement with the data.[68] The reason that the result obtained from the calculation of Ref. 47 underestimates the ^{3}H(γ,n) cross section below its peak is not understood.[68]

The ^{3}H(γ,2n) data of the present measurement are compared in Fig. 13(c) with the calculations of Gibson and Lehman,[68] Levinger and Fitzgibbon,[53] and Vostrikov and Zhukov.[51] The hyperspherical-harmonics calculations[51,53] (those of Ref. 51 were done with Eikemeier-Hackenbroich and super-soft-core potentials) yield cross sections which peak at too high an energy. The shape of the Faddeev-

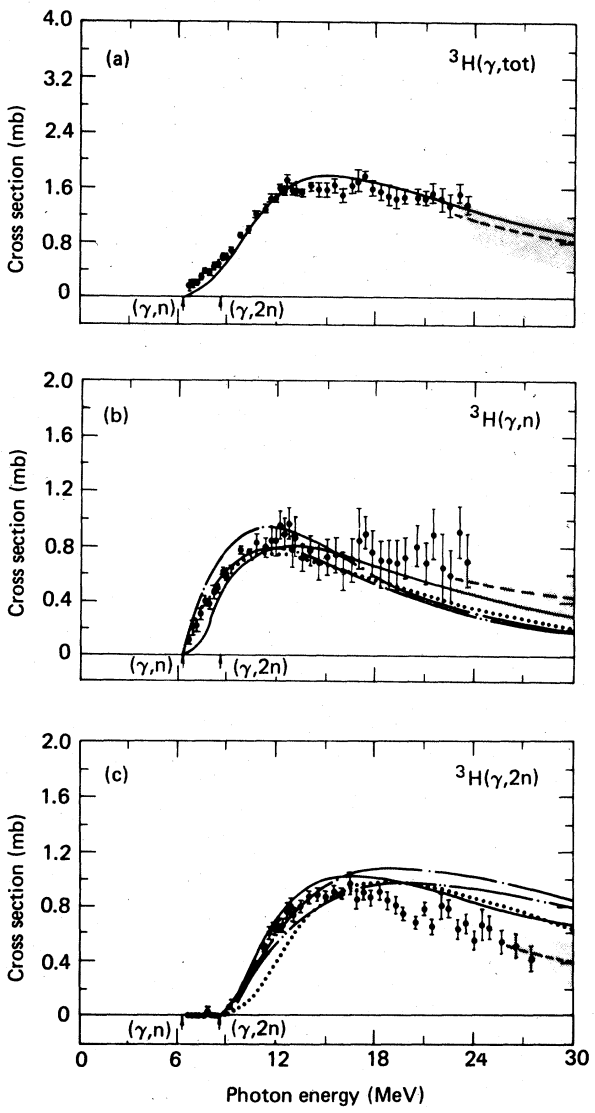

FIG. 13. (a) Total photodisintegration cross section for ^{3}H: filled circles, present data; dashed curve with shaded error band, extrapolation of the present data; solid curve, sum of theoretical predictions for ^{3}H(γ,n) from Ref. 47 and ^{3}H(γ,2n) from Ref. 68. (b) Two-body photodisintegration cross section for ^{3}H: filled circles, present data; dashed curve with shaded error band, extrapolation of the present data; solid curve, theoretical prediction from Ref. 47; dash-dot-dash curve, theoretical prediction from Ref. 33; dash-dot-dot-dash curve and dotted curve, theoretical predictions from Ref. 39. (c) Three-body photodisintegration cross section for ^{3}H: filled circles, present data; dashed curve with shaded error band, extrapolation of the present data; solid curve, theoretical prediction from Ref. 68; dash-dot-dash curve and dash-dot-dot-dash curves, theoretical predictions from Ref. 51; dotted curve, theoretical prediction from Ref. 53.

method result[68] (solid curve) agrees better with the data, but the experimental cross section is a bit smaller at its peak and decreases slightly faster in the energy region above the peak. The results of the calculation of Gibson and Lehman should agree better with the ^{3}H(γ,2n) data than with the ^{3}He(γ,n) data [Fig. 12(c)], because the Coulomb repulsion between the outgoing protons for the latter reaction is not included in their model, but they do not. However, the agreement between the theoretical results of Gibson and Lehman and the present data probably would be improved, especially in the region below the peak of the cross section (where the experimental data are least subject to systematic errors), if tensor forces were included in the interaction model and if the S' state were not excluded from the ground-state wave function.

The data points and the dashed line with the shaded error band shown in Fig. 13(a) represent the total cross section for the photodisintegration of ^{3}H. These experimental results were obtained by adding together the ^{3}H(γ,n) and ^{3}H(γ,2n) results of this experiment. The error flags assigned to the data points have been corrected for the correlation between the (γ,n) and the (γ,2n) reactions through the multiplicity correction; this correction reduces somewhat the magnitude of the error flags compared to that which would be obtained by adding the statistical errors in quadrature. For the case of ^{3}H(γ,2n), the results were extended to 30 MeV with the extrapolation shown as the dashed curve in Fig. 13(c). The shaded band in Fig. 13(c) represents the uncertainty for this extension. The extrapolation for the case of ^{3}H(γ,n) is the result of a compromise between the present data and the lower-lying data of Ref. 34; the dashed line and shaded error band in Fig. 13(b) were chosen to represent this compromise extension. The data for the ^{3}H total cross section are compared in Fig. 13(a) with the theoretical result of Gibson and Lehman,[48,68] which was constructed from the predictions of their calculations for the two- and three-body breakup. Good agreement with the data is seen despite the limitations of the model.

C. Integrated cross sections and sum rules

The integrated cross sections and their first and second moments for the reactions ^{3}He(γ,n), ^{3}H(γ,n), and ^{3}H(γ,2n) are given in Table III. The uncertainties attached to the values shown in Table III are dominated by the systematic (rather than the statisti-

TABLE III. Integrated cross sections and moments.

Reaction	$E_{\gamma_{max}}$ (MeV)	σ_{int} (MeV mb)[a]	σ_{-1} (mb)[b]	σ_{-2} (mb MeV^{-1})[c]
^{3}He(γ,n)	23.4	12.3 ± 1.2	0.760 ± 0.061	0.050 ± 0.004
^{3}H(γ,n)	23.4	11.7 ± 1.2	0.840 ± 0.067	0.067 ± 0.005
^{3}H(γ,2n)	23.4	10.2 ± 1.0	0.638 ± 0.051	0.042 ± 0.003
^{3}He(γ,n)	25.8	14.1 ± 1.4	0.833 ± 0.067	0.053 ± 0.004
^{3}H(γ,n)[d]	25.8	13.2 ± 1.3	0.896 ± 0.072	0.069 ± 0.006
^{3}H(γ,2n)	25.8	11.5 ± 1.2	0.691 ± 0.055	0.044 ± 0.003
^{3}He(γ,n)[d]	26.4	14.4 ± 1.4	0.850 ± 0.068	0.053 ± 0.004
^{3}H(γ,n)[d]	26.4	13.6 ± 1.3	0.900 ± 0.072	0.070 ± 0.006
^{3}H(γ,2n)	26.4	12.0 ± 1.2	0.709 ± 0.057	0.045 ± 0.004
^{3}He(γ,n)[d]	30.0	16.4 ± 2.0	0.917 ± 0.092	0.056 ± 0.004
^{3}H(γ,n)[d]	30.0	15.4 ± 1.8	0.986 ± 0.099	0.072 ± 0.006
^{3}H(γ,2n)[d]	30.0	13.6 ± 1.6	0.767 ± 0.077	0.047 ± 0.004

[a] $\sigma_{int} = \int_0^{E_{\gamma_{max}}} \sigma(E_\gamma) dE_\gamma$.

[b] $\sigma_{-1} = \int_0^{E_{\gamma_{max}}} \sigma(E_\gamma) E_\gamma^{-1} dE_\gamma$.

[c] $\sigma_{-2} = \int_0^{E_{\gamma_{max}}} \sigma(E_\gamma) E_\gamma^{-2} dE_\gamma$.

[d] Extrapolated (from the present data only).

cal) uncertainties of the experiment. The three reactions are compared at several values for the upper limit of integration $E_{\gamma_{max}}$, corresponding to the highest-energy data point for each reaction, and also for $E_{\gamma_{max}} = 30$ MeV. For all values of $E_{\gamma_{max}}$, the values for the reaction ^{3}H(γ,n) are larger than the values for ^{3}H(γ,2n). Primarily because of the difference in thresholds, the integrated cross section for the reaction ^{3}He(γ,n) is larger than that for the reaction ^{3}H(γ,n), while the energy-weighted integrated cross sections for ^{3}H(γ,n) are larger than those for ^{3}He(γ,n).

The absence of data at higher energies and the simple models for which the sum rules were derived (see below) reduce the value of a comparison of sum-rule calculations with the present results. Integration of the present cross-section results (and extrapolation) for ^{3}He(γ,n) up to 30 MeV yields a value of 16.4 ± 2.0 MeV mb. The cross-section results for ^{3}He(γ,d) from Ref. 17, when integrated up to the same energy, yield a value of 11.8 ± 1.2 MeV mb. The value for the integrated total photodisintegration cross section σ_{int} for ^{3}He is thus 28.2 ± 2.8 MeV mb at 30 MeV, which is comparable to the corresponding ^{3}H value for σ_{int} of 29.0 ± 3.0 MeV mb (also obtained with some extrapolation). These values for σ_{int} are only ~40% of the strength predicted by Drechsel and Kim[71] for the entire three-body photodisintegration cross section integrated up to the pion threshold. The first moment of the integrated total cross section σ_{-1} for ^{3}He up to 30 MeV, obtained from the combined results of the present measurement and of Ref. 17, is 1.74 ± 0.17 mb, while the present result for ^{3}H is 1.75 ± 0.18 mb. These values for σ_{-1} are ~80% of the strength predicted by the sum rule of O'Connell and Prats.[72] It should be noted here that neither of these calculations differentiates between ^{3}H and ^{3}He because both assume charge symmetry to hold.

The form of the sum rule for σ_{-1} derived by O'Connell and Prats[72] which contains *no* assumption of charge symmetry is

$$\sigma_{-1} = \tfrac{2}{3}\pi^2\alpha(3r_m^2 - r_v^2) ,$$

where α is the fine-structure constant. The mean-square nuclear-matter and isovector radii are given, respectively, by

$$3r_m^2 = 2r_L^2 + r_0^2$$

and

$$r_v^2 = 2r_L^2 - r_0^2 ,$$

where r_L and r_0 are the radii of the like and odd nucleons, respectively, for both ^{3}H and ^{3}He. The resulting expression $\sigma_{-1} = \frac{4}{3}\pi^2\alpha r_0^2$ can be used to compute values for σ_{-1} from the measured charge and magnetic radii r_{ch} and r_{mag}, since $r_0^2(^3\text{H}) = r_{ch}^2(^3\text{H}) - r_{ch}^2(^1\text{H}) = 2.15 \pm 0.05$ fm^2 and $r_0^2(^3\text{He}) = r_{mag}^2(^3\text{He}) - r_{mag}^2(n) = 3.04 \pm 0.05$ fm^2 from the results of Ref. 4 [$r_{ch}(^3\text{H}) = 1.70 \pm 0.05$ fm], Ref. 5 [$r_{mag}(^3\text{He}) = 1.935 \pm 0.04$ fm], Ref. 73 [$r_{ch}(^1\text{H}) = 0.862 = 0.012$ fm], and Ref. 74 [$r_{mag}(n) = 0.84 \pm 0.03$ fm]. Thus the sum rule predicts that $\sigma_{-1}(^3\text{H}) = 2.06 \pm 0.07$ mb and $\sigma_{-1}(^3\text{He}) = 2.92 \pm 0.07$ mb, compared to the experimental results integrated up to 30 MeV of $\sigma_{-1}(^3\text{H}) = 1.75 \pm 0.18$ mb and $\sigma_{-1}(^3\text{He}) = 1.74 \pm 0.17$ mb (see above).

Experimental results extending up to the pion-production threshold also would be useful in this regard. In spite of the limited energy range for the present experimental results, however, it can be seen, because some of the experimental uncertainties cancel in their ratio, that the sum-rule predictions for $\sigma_{-1}(^3\text{He})/\sigma_{-1}(^3\text{H})$ exceed significantly (by 40%) the experimental ratio. This means either that the sum rule [which is based only upon (a simplified form for) the ground-state wave functions of the trinucleons] is invalid or that charge symmetry does not hold here. Again, it should be noted that if the choice of the upper set of data from Ref. 17 (or the data of Ref. 29) were used for the ^{3}He(γ,d) cross section, this disagreement would be reduced (but only by about half its magnitude). In any case, it is clear that more theoretical effort must be channeled into sum-rule calculations that take into account more refined ground-state wave functions before a quantitative value for any charge asymmetry can be inferred.

D. Photodisintegration cross sections and charge symmetry

The two- and three-body cross sections for ^{3}H and ^{3}He are compared in Figs. 14(a) and (b), respectively, after shifting the data in energy in order to account for the different reaction thresholds. The cross sections shown in Fig. 14 were synthesized from all the available experimental data and therefore do not represent the results of this experiment alone, although these latter were weighted the most heavily. For ^{3}He(γ,n) in particular [Fig. 14(b)], the results of Ref. 30 were given less weight than those of the others below ~ 15 MeV because the latter agree well with each other, and the results of Ref. 31 were given less weight above ~ 18 MeV because of the questionable neutron-detector efficiency used (see above). Also, no attempt was made to include structure in this representation of the ^{3}He(γ,n) cross section.

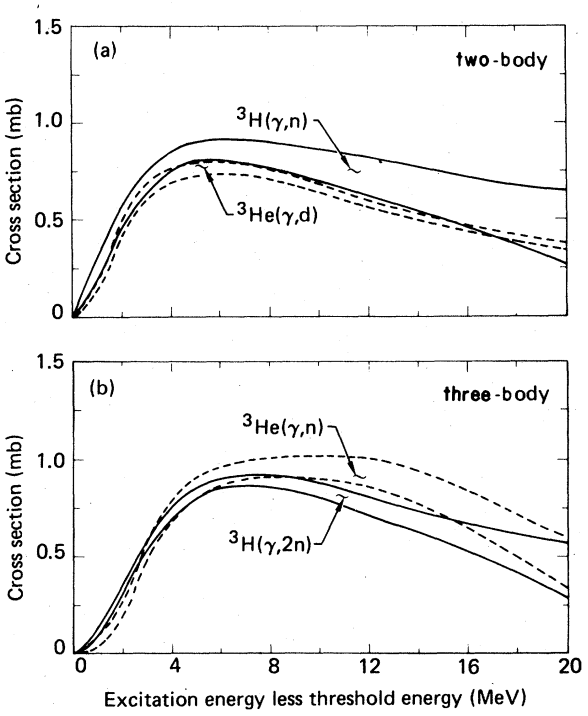

FIG. 14. (a) Experimental two-body photodisintegration cross sections for ^{3}H (represented by the region bounded by the solid curves) and for ^{3}He (the region bounded by the dashed curves). (b) Experimental three-body photodisintegration cross sections for ^{3}H (represented by the region bounded by the solid curves) and ^{3}He (the region bounded by the dashed curves). Note that the cross-section data for both (a) and (b) have been corrected for the different reaction thresholds by plotting them as functions of excitation energy less threshold energy.

Particular attention should be given to comparing the cross sections in the energy region from threshold up to their peaks, where the systematic uncertainties are smallest. In Fig. 14(a) the ^{3}H(γ,n) data are seen to lie 10—15 % higher in the peak region than the ^{3}He(γ,d) data, and the two cross sections

are seen to exhibit roughly the same shape. [On the high-energy side of the peak the $^3H(\gamma,n)$ cross section perhaps decreases somewhat less abruptly than does the $^3He(\gamma,d)$ cross section.] The fact that the strengths of the two cross sections at their peaks are different is not in agreement with the theoretical prediction of Gibson and Lehman.[47]

The $^3He(\gamma,n)$ and $^3H(\gamma,2n)$ cross sections of Fig. 14(b) agree in magnitude with each other from about 3 to 6 MeV above their respective thresholds, where the two sets of data are most reliable. At higher energies the $^3He(\gamma,n)$ cross section continues to climb to a higher peak (by about 10%), at a higher energy, than the $^3H(\gamma,2n)$ cross section; the latter decreases more or less monotonically above $E_\gamma - E_{\rm thr} \simeq 8$ MeV. Above its peak at $E_\gamma - E_{\rm thr} \simeq 12$ MeV, the $^3He(\gamma,n)$ cross section decreases more sharply than that for $^3H(\gamma,2n)$. These two cross sections also have quite different shapes just above threshold, where the $^3H(\gamma,2n)$ cross section increases markedly more rapidly than does the $^3He(\gamma,n)$ cross section.

The total photodisintegration cross sections for the two trinucleon systems, shown in Fig. 15, are seen to be very much the same except just above threshold where their different behavior can be noted. That this is so shows that the rather substantial differences in the partial cross sections (see Fig. 14) are largely compensated in the sum; this striking result could not have been anticipated in the absence of the present measurements.

It should be noted here, however, that if the data from the upper group of cross-section data points of Ref. 17 were chosen to represent the $^3He(\gamma,d)$ cross section (recall that we have chosen the lower group), then the difference in magnitude observed between the $^3H(\gamma,n)$ and $^3He(\gamma,d)$ [see Fig. 14(a)] cross sections would be much less notable and, in fact, would largely disappear. Then, however, the total photodisintegration cross sections for ^3H and ^3He (Fig. 15) would be appareciably different, with the one for ^3He being the larger.

Since the observed difference between the two three-body breakup cross sections near threshold probably is real and not an artifact produced by poor statistics or systematic uncertainties, then this effect could be attributed to Coulomb effects in ^3He, which might be large just above threshold. On the other hand, despite the fact that the *p-d* system in ^3He is affected by Coulomb repulsion near threshold, the enhancement [see Fig. 14(a)] of the $^3H(\gamma,n)$ cross section over the $^3He(\gamma,d)$ cross section at higher energies is unexpected.[47] The same can be said for the enhancement of the $^3He(\gamma,n)$ cross section over the $^3H(\gamma,2n)$ cross section. Perhaps most of these differences can be explained as effects of the final-state interactions. If not, they must be ascribed to differences in the ground-state wave functions for the two mirror trinucleons. In order to address this issue, further theoretical work using exact models which include both the Coulomb repulsion between charged nucleons and the tensor part of the nucleon-nucleon interaction should be pursued. Only then can one ascertain whether the significant differences between the partial cross sections can be accounted for by electromagnetic effects alone.

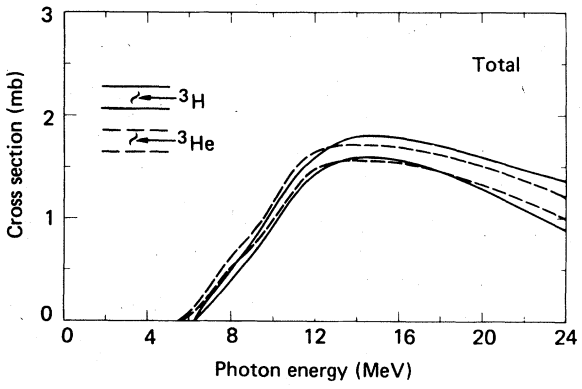

FIG. 15. Experimental total photodisintegration cross sections for ^3H (represented by the region bounded by the solid curves) and ^3He (the region bounded by the dashed curves), plotted as a function of photon energy.

V. CONCLUSIONS

More theoretical work will be needed before the experimental results for the photodisintegration of three-body nuclei can test quantitatively the charge symmetry of the nuclear interaction. The present theoretical models are still rudimentary in that they do not include simultaneously a consistent treatment of the final-state interactions, S' and D components in the ground-state wave function, the tensor force in the triplet interaction, and the Coulomb repulsion between the protons in ^3He. Both the strong and the electromagnetic interactions seem to contribute to the distribution of strength between the two- and three-body breakup channels of ^3He, but the theory does not quantify the magnitude of the electromagnetic contribution to the cross-section strengths of the two breakup modes. As a consequence of these problems, the agreement between the experimental

and theoretical results is, in the mean, not notably good. The contrast in the threshold behavior of the ^{3}H and ^{3}He three-body breakup cross sections (that for ^{3}H rises much faster than that for ^{3}He) seems too extreme to be the effect of the Coulomb force alone, but lacks any other theoretical explanation. Perhaps the more significant problem for the theorists, however, is the explanation of the different distribution of cross-section strength between the two- and three-body breakup channels observed for ^{3}H and ^{3}He.

One would think that the similarity of the integrated total cross sections and the integrated energy-weighted cross sections for ^{3}H and ^{3}He could be understood, through the sum rules, as a consequence of the principle of charge symmetry; however, this inference is brought into question by the large difference in the odd-nucleon radii for these nuclei. A better calculation is needed to bestow more credibility upon the sum-rule predictions which up to the present time do not distinguish between ^{3}H and ^{3}He photodisintegration. In summary, the results of the present photodisintegration measurements constitute a new challenge to the principle of charge symmetry for the trinucleon system; but more work is needed to ascertain whether these experimental results can be explained entirely by a more complete theoretical treatment.

ACKNOWLEDGMENTS

We are pleased to acknowledge the technical assistance of Dr. R. A. Alvarez and Dr. J. G. Woodworth and the theoretical guidance of Dr. A. Goldberg and especially of Dr. B. F. Gibson, to whom thanks are due as well for his providing us with extensive calculational output prior to publication. We also thank Dr. M. Fabre de la Ripelle for sending us his calculational results prior to publication. This work was performed at Lawrence Livermore Laboratory under the auspices of the U. S. Department of Energy under Contract No. W-7405-ENG-48. Previous reports of part of this work have appeared as Refs. 75–78. Further details can be found in Ref. 79.

[1]J. S. Levinger, in *Springer Tracts in Modern Physics: Nuclear Physics,* edited by G. Höhler (Springer, New York, 1974), Vol. 71, p.88.

[2]R. A. Brandenberg, S. A. Coon, and P. U. Sauer, Nucl. Phys. A294, 305 (1978).

[3]J. L. Friar and B. F. Gibson, Phys. Rev. C 18, 908 (1978).

[4]H. Collard, R. Hofstadter, E. B. Hughes, A. Johansson, M. R. Yearian, R. B. Day, and R. T. Wagner, Phys. Rev. 138, B57 (1965).

[5]P. Dunn, Ph.D. thesis, Harvard University, 1980 (unpublished); see as well the earlier paper of J. S. McCarthy, I. Sick, and R. R. Whitney, Phys. Rev. C 15, 1396 (1977).

[6]R. G. Sachs, in *Nuclear Theory* (Addison-Wesley, Cambridge, Massachusetts, 1953), p.180.

[7]P. Marmier and E. Sheldon, in *Physics of Nuclei and Particles* (Academic, New York, 1970), Vol. 2, p.919.

[8]A. N. Gorbunov, in *Photonuclear and Photomesic Processes,* Proceedings of the P. N. Lebedev Physics Institute, edited by D. V. Skobel'tsyn (Nauka, Moscow, 1974), Vol. 71, p.1; (Consultants Bureau, New York, 1976), Vol. 71, p.1 (translation).

[9]M. S. Weiss, in *Interaction Studies in Nuclei,* edited by H. Jochim and B. Ziegler (North-Holland, Amsterdam, 1975), p.599.

[10]C. Ciofi degli Atti, in *Photonuclear Reactions I,* edited by S. Costa and C. Schaerf (Springer, New York, 1977), p.521.

[11]B. L. Berman, L. J. Koester, Jr., and J. H. Smith, Phys. Rev. Lett. 10, 527 (1963); Phys. Rev. 133, B117 (1964).

[12]A. N. Gorbunov and A. T. Varfolomeev, Phys. Lett. 5, 149 (1963); V. N. Fetisov, A. N. Gorbunov, and A. T. Varfolomeev, Nucl. Phys. 21, 305 (1965).

[13]E. Finckh, R. Kosiek, K. H. Lindenberger, U. Meyer-Berkhout, N. Nücker, and K. Schlüpmann, Phys. Lett. 7, 271 (1963).

[14]C. Becchi, G. E. Manuzio, L. Meneghetti, and S. Vitale, Phys. Lett. 8, 322 (1964).

[15]J. R. Stewart, R. C. Morrison, and J. S. O'Connell, Phys. Rev. 138, B372 (1965).

[16]N. M. O'Fallon, L. J. Koester, Jr., and J. H. Smith, Phys. Rev. C 5, 1926 (1972).

[17]G. Ticcioni, S. N. Gardiner, J. L. Matthews, and R. O. Owens, Phys. Lett. 46B, 369 (1973).

[18]J. B. Warren, K. L. Erdman, L. P. Robertson, D. A. Axen, and J. R. MacDonald, Phys. Rev. 132, 1691 (1963).

[19]S. K. Kundu, Y. M. Shin, and G. D. Wait, Nucl. Phys. A171, 384 (1971).

[20]D. M. Skopik and Y. M. Shin, Can. J. Phys. 50, 392 (1972).

[21]C. C. Chang, W. R. Dodge, and J. J. Murphy II, Phys. Rev. C 9, 1300 (1974).

[22]D. M. Skopik, J. J. Murphy II, Y. M. Shin, K. F. Chong, and E. L. Tomusiak, Phys. Rev. C 11, 693 (1975).

[23]G. M. Griffiths, E. A. Larson, and L. P. Robertson, Can. J. Phys. 40, 402 (1962).
[24]W. Wölfli, R. Bösch, J. Lang, R. Müller, and P. Marmier, Helv. Phys. Acta 22, 75 (1966); Phys. Lett.. 40, 946 (1967).
[25]A. van der Woude, M. L. Halbert, C. R. Bingham, and B. D. Belt, Phys. Rev. Lett. 26, 909 (1971).
[26]C. C. Chang, E. M. Diener, and E. Ventura, Phys. Rev. Lett. 29, 307 (1972).
[27]M. L. Halbert, P. Paul, K. A. Snover, and E. K. Warburton, in *Procedings of the International Conference of Few-Particle Problems in the Nuclear Interaction, Los Angeles, California, 1972,* edited by I. Slaus, S. A. Moskowski, R. P. Haddock, and W. T. H. van Oers (North-Holland, Amsterdam, 1973), p.525.
[28]J. L. Matthews, T. Kruse, M. E. Williams, R. O. Owens, and W. Savin, Nucl. Phys. A223, 221 (1974).
[29]D. M. Skopik, H. R. Weller, N. R. Roberson, and S. A. Wender, Phys. Rev. C 19, 601 (1979).
[30]H. M. Gerstenberg and J S. O'Connell, Phys. Rev. 144, 834 (1961).
[31]B. L. Berman, S. C. Fultz, and P. F. Yergin, Phys. Rev. C 10, 2221 (1974).
[32]M. Cerineo, K. Ilakovac, I. Slaus, and P. Tomas, Phys. Rev. 124, 1947 (1961).
[33]R. Bösch, J. Lang, R. Müller, and W. Wölfli, Phys. Lett. 8, 120 (1964); Helv. Phys. Acta 38, 753 (1965).
[34]R. Kosiek, D. Müller, R. Pfeiffer, and O. Merwitz, Phys. Lett. 21, 199 (1966); R. Pfeiffer, Z. Phys. 208, 129 (1968).
[35]M. Verde, Helv. Phys. Acta 23, 453 (1950); Nuovo Cimento 7, 283 (1950).
[36]L. I. Schiff, Phys. Rev. 52, 242 (1937).
[37]J. C. Gunn and J. Irving, Philos. Mag. 42, 1353 (1951).
[38]U. Eichmann, Z. Phys. 175, 115 (1963).
[39]M. Rahman, H. M. Sen Gupta, and D. Hussain, Nucl. Phys. A168, 314 (1971).
[40]L. D. Faddeev, Zh. Eksp. Teor. Fiz. 39, 1459 (1960) [Sov. Phys.—JETP 12, 1014 (1961)].
[41]A. N. Mitra, Nucl. Phys. 32, 529 (1962).
[42]Yoshio Yamaguchi, Phys. Rev. 95, 1628 (1954); Yoshio Yamaguchi and Yoriko Yamaguchi, *ibid.* 95, 1635 (1954).
[43]I. M. Barbour and A. C. Phillips, Phys. Rev. Lett. 19, 1388 (1967).
[44]I. M. Barbour and A. C. Phillips, Phys. Rev. C 1, 165 (1970).
[45]I. M. Barbour and J. E. Hendry, Phys. Lett. 38B, 151 (1972).
[46]J. E. Hendry and A. C. Phillips, Nucl. Phys. A211, 533 (1973).
[47]B. F. Gibson and D. R. Lehman, Phys. Rev. C 11, 29 (1975).
[48]B. F. Gibson and D. R. Lehman, Phys. Rev. C 13, 477 (1976).
[49]D. R. Lehman, F. Prats, and B. F. Gibson, Phys. Rev. C 19, 310 (1979).
[50]L. M. Delves, Nucl. Phys. 29, 268 (1962).
[51]A. N. Vostrikov and M. V. Zhukov, Yad. Fiz. 26, 716 (1977) [Sov. J. Nucl. Phys. 26, 377 (1977)].
[52]K. K. Fang, J. S. Levinger, and M. Fabre de la Ripelle, Phys. Rev. C 17, 24 (1978).
[53]J. S. Levinger and R. Fitzgibbon, Phys. Rev. C 18, 56 (1978).
[54]B. L. Berman and S. C. Fultz, Rev. Mod. Phys. 47, 713 (1975).
[55]J. G. Woodworth, K. G. McNeill, J. W. Jury, R. A. Alvarez, B. L. Berman, D. D. Faul, and P. Meyer, Lawrence Livermore Laboratory Report No. UCRL-77471, 1978; Phys. Rev. C 19, 1667 (1979).
[56]J. T. Caldwell, Ph.D thesis, Lawrence Livermore Laboratory Report No. UCRL-50287, 1967 (unpublished).
[57]B. L. Berman, J. T. Caldwell, R. R. Harvey, M. A. Kelly, R. L. Bramblett, and S. C. Fultz, Phys. Rev. 162, 1098 (1967).
[58]J. Kimlinger and E. Plechaty, Lawrence Livermore Laboratory Report No. UCRL-50400, Vol. 14, 1976 (unpublished).
[59]E. A. Davis, T. W. Bonner, D. W. Worley, Jr., and R. Bass, Nucl. Phys. 48, 169 (1963).
[60]T. W. Phillips, B. L. Berman, and J. D. Seagrave, Phys. Rev. C 22, 384 (1980).
[61]B. L. Berman *et al.,* LLL Operational Safety Procedure 194, Suppl. 23, 1978 (unpublished).
[62]J. W. Jury, B. L. Berman, D. D. Faul, P. Meyer, and J. G. Woodworth, Phys. Rev. C 21, 503 (1980).
[63]R. L. Bramblett, J. T. Caldwell, R. R. Harvey, and S. C. Fultz, Phys. Rev. 133, B869 (1964); J. T. Caldwell, R. L. Bramblett, B. L. Berman, R. R. Harvey, and S. C. Fultz, Phys. Rev. Lett. 15, 976 (1965).
[64]J. Ahrens, H. B. Eppler, H. Gimm, M. Kronig, P. Riehn, A. Ziegler, and B. Ziegler, Phys. Lett. B52, 43 (1974).
[65]G. Breit, in *Proceedings of the International Conference on Photonuclear Reactions and Applications, Asilomar, California, 1973,* edited by B. L. Berman (Lawrence Livermore Laboratory, Livermore, 1973), p.323.
[66]B. L. Berman, D. D. Faul, P. Meyer, and D. L. Olson, Phys. Rev. C 22, 2273 (1980); Lawrence Livermore Laboratory Report No. UCRL-82188, 1980.
[67]R. A. Alvarez, B. L. Berman, D. D. Faul, F. H. Lewis, Jr., and P. Meyer, Phys. Rev. C 20, 128 (1979).
[68]B. F. Gibson and D. R. Lehman, private communication.
[69]J. M. Hendry and A. M. Macleod, J. Phys. G 1, 528 (1975).
[70]J. B. Ballot and M. Fabre de la Ripelle, Université Paris-Sud, Institut de Physique Nucléaire Report No. IPNO/TH 79-12, 1979 (unpublished).
[71]D. Drechsel and Y. E. Kim, Phys. Rev. Lett. 40, 531 (1978).
[72]J. S. O'Connell and F. Prats, Phys. Rev. 184, 1007 (1969).
[73]G. G. Simon, Ch. Schmitt, F. Borkowski, and V. H.

Walther, Nucl, Phys. A333, 381 (1980).
[74]G. Höhler, E. Pietarinen, I. Sabba-Stefanescu, F. Borkowski, G. G. Simon, V. H. Walther, and R. D. Wendling, Nucl. Phys. B114, 505 (1976).
[75]D. D. Faul, P. Meyer, D. L. Olson, and B. L. Berman, Bull. Am. Phys. Soc. 24, 647 (1979).
[76]P. Meyer, D. D. Faul, D. L. Olson, and B. L. Berman, Bull. Am. Phys. Soc. 24, 647 (1979).
[77]B. L. Berman, D. D. Faul, P. Meyer, and D. L. Olson, in *Nuclear Physics with Electromagnetic Interactions,* edited by H. Arenhövel and D. Drechsel (Springer, New York, 1979), p.403.
[78]D. D. Faul, B. L. Berman, P. Meyer, and D. L. Olson, Phys. Rev. Lett. 44, 129 (1980).
[79]D. D. Faul, Ph.D. thesis, Lawrence Livermore Laboratory, Report No. UCRL-53057, 1980 (unpublished).